Advanced Composites and Hybrid Materials (2022) 5:2847–2872
https://doi.org/10.1007/s42114-022-00467-6

ORIGINAL RESEARCH

Biodegradable and injectable poly(vinyl alcohol) microspheres in silk sericin-based hydrogel for the controlled release of antimicrobials: application to deep full-thickness burn wound healing

Bianza Moise Bakadia[1,2] · Aimei Zhong[3] · Xiahong Li[4] · Biaou Oscar Ode Boni[1] · Abeer Ahmed Qaed Ahmed[5] · Tiatou Souho[6] · Ruizhu Zheng[1] · Zhijun Shi[1] · Dingwen Shi[8] · Lallepak Lamboni[1,7] · Guang Yang[1]

Received: 8 February 2022 / Revised: 4 April 2022 / Accepted: 11 April 2022 / Published online: 7 May 2022

Abstract

Deep full-thickness burn wounds are prone to multi-drug resistant (MDR) infections following injury, which extends the healing time. Thus, providing a bioactive hydrogel dressing with prolonged antimicrobial activity and reduced dressing changes is quite desirable for accelerating burn wound healing and preventing scarring. To achieve this, we developed an injectable hydrogel based on silk sericin (SS), poly(vinyl alcohol) (PVA), and PVA microspheres (MSs) containing vancomycin (VA), gentamicin (GEN), or their association (VG) for the healing of infected burn wounds. The microspheres were prepared by inverse emulsion crosslinking, while the hydrogels were prepared by freeze-thawing cycles. Antibacterial studies showed that gentamicin acts synergistically with vancomycin by increasing the bacterial killing rate and enhancing the biofilm inhibition and eradication effects on methicillin-resistant *Staphylococcus aureus* more than on *Pseudomonas aeruginosa* and *Escherichia coli*. Findings from FESEM images showed that the microspheres were sphere-shaped with a smooth surface and their average diameter ranging from 26.22 to 32.42 µm suitable for parenteral drug delivery. The prepared hydrogel containing 10% of microspheres was more elastic than viscous, with lower tan delta values (< 1) suited for deeper injection with homogeneous tissue integration. The incorporation of VG-PVAMS in the PVA/SS hydrogel led to zero-order release kinetics and efficient antimicrobial effects. Moreover, the in vivo study using a rat full-thickness burn model showed that the VG-PVAMS@PVA/SS hydrogel displays a better therapeutic effect than drug-free PVAMS@PVA/SS hydrogel and Tegaderm™ film dressing by inducing early vascularization and collagen deposition, leading to early re-epithelialization and burn wound closure.

Keywords Antimicrobial dressing · Burn wound healing · Silk sericin · Controlled release · Microspheres · Injectable hydrogel

1 Introduction

The skin is the largest and most complex organ of the human body. Involved in the innate immune defense, it is a multilayer barrier that effectively protects the body against penetration of foreign substances originating from the external environment that it directly relates to [1]. It is exposed to numerous injuries, among which burns constitute a public health problem. A deep burn of the skin causes immune depression at the cutaneous and mucosal barrier levels, resulting in infectious complications that generate a heavy economic and social burden due to their recurrence and morbidity, which further increases death risks [2].

The burn wound, germ-free, in the first hours post-burning, is in fact promptly colonized (within 48 h) by cutaneous

Bianza Moise Bakadia and Aimei Zhong contributed equally to this work.

Highlights
- Poly(vinyl alcohol) (PVA)/silk sericin (SS) hydrogels loaded with vancomycin–gentamicin/PVA microspheres were synthesized.
- Vancomycin and gentamicin exhibited a synergistic antibacterial effect in loaded hydrogels.
- The biological properties of the hydrogels improved obviously with microsphere loading.
- The microsphere hydrogel exhibited sustained drug release, antibacterial activity, and excellent cytocompatibility.
- The microsphere hydrogel system accelerates full-thickness burn wound healing.

Extended author information available on the last page of the article

microorganisms (predominantly Gram-positive bacteria) and then (by the end of the first week) by mainly Gram-negative bacteria or fungi of digestive, respiratory, or environmental origins [3, 4]. Afterward, the burn wound can be colonized by resistant microorganisms, including methicillin-resistant *Staphylococcus aureus* (MRSA), multi-drug resistant (MDR) *Pseudomonas,* and vancomycin-resistant *Enterococcus* (VRE) [5]. In infected burn wounds, germs preferentially lodge at the junction between the burned zone and the adjacent healthy zone, where they find a moist, warm, and protein-rich environment conducive to microbial development, whereas the weak vascularity that limits the influx of immune cells allows microbial escape from the immune system and antibiotics [3, 4]. The rapidly growing microbial population then contributes to the maceration of the burned area and destruction of unburned skin tissue [6]. Moreover, burn injuries often develop eschars that cover the wound and create a favorable environment for microbial growth [3, 4]. Fortunately, the use of topical antimicrobials and adequate dressings can enable wound cleaning and clearance of infectious contaminants. However, the pathophysiology of deep burn is still not fully understood, challenging the design of effective dressings and therapeutic strategies [7].

Wound dressings are biomaterials with an important role in the treatment of skin wounds. They promote the regeneration of neotissue and, at the same time, prevent infections during long-term treatment [8]. Among biomaterials, hydrogels, particularly injectable ones that can perfectly adapt to the wound shape, are usually preferred for the management of burn wounds, due to their high water content and also their swelling ability, great porosity, soft consistency, biocompatibility, and morphological similarity with natural tissues [7, 8]. For improved biological responses, hydrogels are enriched with drugs incorporated into nanoparticles [9, 10], nanofibers [11, 12], nanofiber nanoparticle assemblies [13], microspheres, microsponges, or liposomes as carriers [14–16]. Compared to microspheres, liposomes provide a relatively low rate of drug encapsulation efficiency (around 30%) and turn out to be expensive because of their requirement for ultra-pure materials [17]. In fact, though the cost of their formulations is a major stumbling block to their therapeutic applications in wound healing [18], nanomaterials have a positive impact on wound healing at every stage [18]. Additionally, nanoparticles have a higher surface area [13], resulting in a faster dissolving rate, faster absorption, and enhanced bioavailability compared to microparticles [19]. Similarly, nanofibers are particularly prone to hydrolytic degradation due to their huge surface area-to-volume ratio, which could result in a faster rate of degradation than microfibers [13, 20]. Interestingly, embedding drug-encapsulating microspheres or nanofiber nanoparticles within a hydrogel matrix yields enhanced control of the sustained drug release compared to the use of individual vehicles [13, 21]. Among the different types of carriers, microspheres stand out by providing advantageous drug stability [22]. For their fabrication, both natural and synthetic polymers can be used [23, 24]. Herein, the microspheres were obtained from a widely applied and biocompatible synthetic polymer, poly (vinyl alcohol) (PVA).

PVA is a hydrosoluble synthetic polymer with a semi-crystalline structure. Its composites are used in a variety of biomedical fields, including contact drug delivery systems and wound dressings [25]. It presents good biological and physical properties, namely non-toxicity, non-carcinogenicity, biodegradability, and swelling properties [25]. Thanks to its numerous hydrophilic functional groups, PVA can be mixed with silk sericin (SS) to improve its biological properties. SS is a protein containing essential amino acids and an elevated content of hydrophilic amino acids, particularly serin, which makes it water-soluble [26]. Biocompatibility, antibacterial, UV absorbency, high moisture absorbency, antioxidant, anticoagulase, anti-wrinkle, moisturizing, and whitening properties constitute the main qualities of SS [26]. Hence, as a functional degradable biomaterial, SS is often used as a polymer in association with other polymers for the formation of useful hydrogels [27]. Actually, because of its amorphous nature, SS requires improving its mechanical properties with complementary materials to extend its biomedical application; in this prospect, blending with PVA is one of the best solutions [27].

Antibiotics have been shown to be the most effective antibacterial agents to date, after metal antimicrobials [28]. However, the emergence of antibiotic resistance has become a major obstruction to their progress and application [28]. Thus, it is imperious to develop novel therapeutic approaches that are effective to overcome MDR. As of November 2017, new molecular entity (NME) antibiotics approved by the US FDA were developed to control MDR Gram-negative bacteria included ceftolozane-tazobactam, ceftaroline fosamil, delafloxacin, ceftazidime-avibactam, secnidazole, and meropenem-vaborbactam [29]. In fact, the therapeutic approaches against MDR include antivirulence therapy, antibiotic-adjuvant combination, antibiotic-antibiotic combination, and antibiotic hybrids [29]. Studies have shown that a combination of antibiotics can, to some extent, combat MDR infections as this increases drug potency due to synergistic effects between different drugs [30, 31]. What is more, the combination of antibiotics may lead to the synthesis of an antibiotic hybrid, which is the fusion of different pharmacophores crosslinked into one heteromeric unit expected to retain or increase their biological actions [29, 32]. Approved by the US FDA in September 2020, cefiderocol (ceftazidime + siderophore) is an antibiotic hybrid used for the management of MDR aerobic Gram-negative bacteria [33]. More antibiotic hybrids are under clinical trials, such as cadazolid (ciprofloxacin + tedizolid) against Gram-positive bacteria

and TNP-2092 (ciprofloxacin + rifampin) for treating skin infections, including bacteremia [29].

Therefore, herein, we used vancomycin (VA) and gentamicin (GEN) to fabricate an antimicrobial microsphere based on PVA/SS hydrogel for preventing or fighting burn wound infections, including MRSA infection. VA and GEN are antibacterial drugs that have been approved by the US FDA, and information on their pharmacological properties in clinical development is available. Thus, the time and financial expense of evaluating these drugs in combination form could be reduced.

The therapeutic choices for burn wound infection due to resistant strains such as MRSA are limited. In such cases, VA is the optimal drug for the management of MRSA and resistant *Staphylococcus aureus* (*S. aureus*) infections. VA kills bacteria by inhibiting the development of peptidoglycan, a component of the Gram-positive bacteria cell wall [34]. It can also inhibit the growth of planktonic and biofilm *Candida spp*. [35]. Some strains of *S. aureus* may be VA-intermediate (VISA) or VA–resistant *S. aureus* (VRSA) [34, 36]. Therefore, vancomycin can be combined with other agents, such as GEN, in the expectation of having a greater antimicrobial effect based on a synergistic interaction between the two drugs [37]. GEN is an aminoglycoside that displays bactericidal behavior against a broad spectrum of microorganisms, including MDR *Pseudomonas aeruginosa* (*P. aeruginosa*), *Escherichia coli* (*E. coli*), and *S. aureus.* It acts by binding to ribosomal RNA, which causes the synthesis of abnormal proteins, leading to bacterial death [37].

The originality of this study can be accredited to two features. First, the suggested system uses a biodegradable and injectable PVA/SS hydrogel containing microspheres as a parenteral drug delivery vehicle for sustained delivery of drugs in the burn wound site, which simultaneously enhances cell proliferation and adhesion owing to the incorporation of SS, has prolonged antimicrobial effects due to VA and GEN, and mechanical performance similar to the skin due to the incorporation of PVA. In fact, the concomitant application of sustained antimicrobial delivery in combination with the excellent biocompatible features of PVA and SS is projected to accelerate burn wound healing. Next, this study also investigates the antibacterial interaction between VA and GEN against pathogens involved in burn wound infection. The injectable hydrogel loaded with microspheres was thoroughly characterized for its physicochemical properties, drug release ability, and antimicrobial activity against *P. aeruginosa, E. coli,* and MRSA. Moreover, biological performance was investigated both *in vitro* and *in vivo*. All results show that the microsphere hydrogel containing VA and GEN displays superior antimicrobial activity, thermal stability, higher water uptake, and faster burn wound closure than the drug-free microsphere hydrogel and commercial Tegaderm™ film. Therefore, the study suggests that the microsphere hydrogel containing VA and GEN holds great potential for burn wound healing.

2 Experimental section

2.1 Evaluation of *in vitro* interaction between vancomycin and gentamicin

The time-kill method was used to study the interaction between VA and GEN for all microbial strains used in this study. The antibiotic concentrations used represented the MIC values. A broth culture with no drugs was used as a control. On the basis of the McFarland standard and optical density, the inoculum concentration (10^7 CFU/mL) was determined. Solutions of GEN, VA, and VG were prepared in tubes, and every tube was inoculated (including the control) with the culture of the respective microorganism. Optical density was evaluated at 0, 3, 6, 9, and 24 h after incubation at 37 °C under shaking (50 rpm). Dilutions were prepared as desired for titer determination. Moreover, results were confirmed by colony counts on Mueller Hinton agar (MHA) plates following seeding of the tubes' contents (24 h incubation at 37 °C). Synergism was defined as a decrease in colony counts of at least twofold at 24 h with the mixture of antibiotics compared with that of the most active single antibiotic. The test was implemented in triplicate cultures and was repeated at least 3 times. The values signify the means and standard deviations.

2.2 Preparation of drug-PVA microspheres

Drug-loaded PVA microspheres were prepared by inverse emulsion crosslinking (Fig. 1A). Briefly, PVA solution with a concentration of 6.5% was prepared by dissolving PVA powder in 12 mL of hot distilled water (90 ºC) under magnetic stirring. After it was completely dissolved, the solution was allowed to cool down to room temperature (RT). The antibiotics (VA, GEN, or VG mixture) were thereafter added to the PVA solution at a mass ratio of 15:100. The drug-loaded PVA solution was further stirred until the solution became transparent. The dispersion solution contained 72 mL of liquid paraffin and 2.0% Span 80. The drug-PVA solution was dispersed by adding it in a dropwise manner into the liquid paraffin with magnetic stirring at 600 rpm for 30 min to form water in oil (w/o) dispersion. Afterward, 2.5 mL of glutaraldehyde was added slowly to the medium; five minutes later, 1.5 mL of 1 M HCl was added to the solution as a catalyst. The reaction system was kept at 50 ºC for continued crosslinking for up to 3 h. The microspheres could then be recovered by concentrating them through spinning at 5000 rpm for 10 min. They were thus washed with petroleum ester and ethanol twice each, followed by washing with an

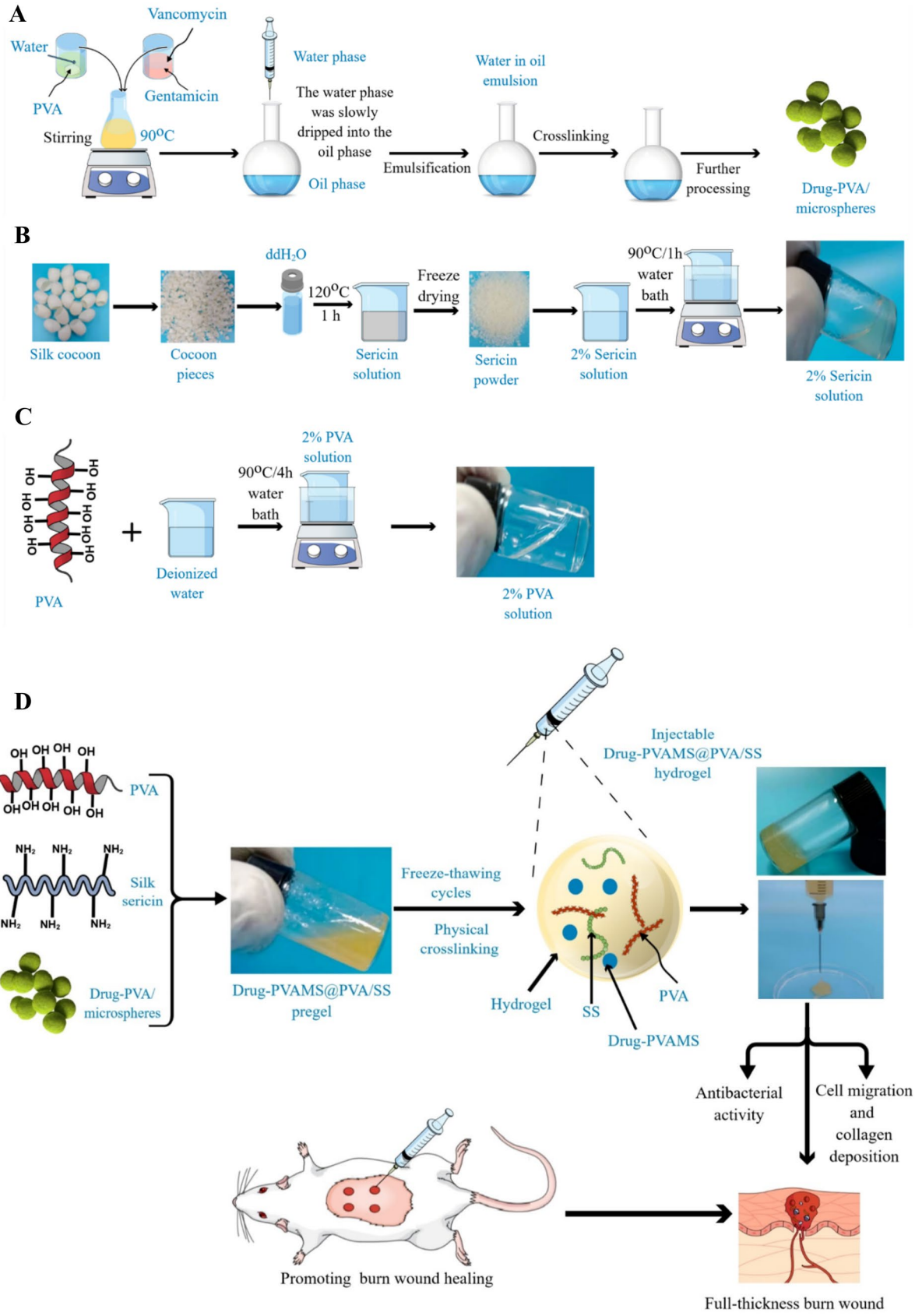
A
Vancomycin
Water
PVA
Gentamicin
Stirring
90°C
Water phase
The water phase was slowly dripped into the oil phase
Oil phase
Emulsification
Water in oil emulsion
Crosslinking
Further processing
Drug-PVA/ microspheres
B
Silk cocoon
Cocoon pieces
ddH2O
120°C 1 h
Sericin solution
Freeze drying
Sericin powder
2% Sericin solution
90°C/1h water bath
2% Sericin solution
C
PVA
Deionized water
90°C/4h water bath
2% PVA solution
2% PVA solution
D
PVA
Silk sericin
Drug-PVA/ microspheres
Drug-PVAMS@PVA/SS pregel
Freeze-thawing cycles
Physical crosslinking
Injectable Drug-PVAMS@PVA/SS hydrogel
Hydrogel
SS
PVA
Drug-PVAMS
Antibacterial activity
Cell migration and collagen deposition
Promoting burn wound healing
Full-thickness burn wound

◂**Fig. 1** Schematic illustration of the preparation of PVAMS@PVA/SS hydrogels with or without gentamicin and vancomycin. (**A**) Preparation of drug-free PVAMS and drug-PVAMS, (**B**) Preparation of silk sericin at 2%, (**C**) Preparation of PVA at 2%, and (**D**) formation of drug-free PVAMS@PVA/SS hydrogel and drug-PVAMS@PVA/SS hydrogel following freeze-thawing cycles, as well as their application for burn wound healing

excess 4% glycine solution to remove the residual glutaraldehyde. The microspheres, including drug-free poly (vinyl alcohol) microsphere (drug-free PVAMS), gentamicin-Poly (vinyl alcohol) microsphere (GEN-PVAMS), vancomycin-poly(vinyl alcohol) microsphere (VA-PVAMS), and vancomycin/gentamicin-Poly (vinyl alcohol) microsphere (VG-PVAMS), were freeze-dried overnight and kept in a desiccator for further use.

2.3 Characterization of PVA microsphere

The microspheres were characterized by Fourier transform infrared (FTIR) spectroscopy, morphological observations, measurements of encapsulation efficiency and drug loading, and antimicrobial activity. For FTIR (VERTEX 70, Bruker, Germany), the microspheres were frozen and dried. The spectra were recorded from 64 scans between 4000 and 400 cm^{-1} with a resolution of 4 cm^{-1}.

The amount of encapsulated drug and drug loading were analyzed by spectrophotometer with the following procedure: A sample of drug-loaded PVAMS was crushed and dissolved in PBS and the mixture was stirred until stabilization of the absorption of the supernatant at 282 nm (the absorption wavelength for VA) or 355 nm (the absorption wavelength for GEN) was achieved. The encapsulation efficiency and drug loading were expressed by Eqs. (1) and (2).

$$\text{Encapsulation efficiency (\%)} = \frac{\text{Mass of drug in microspheres}}{\text{Mass of drug used for microsphere formulation}} \times 100 \quad (1)$$

$$\text{Drug loading (\%)} = \frac{\text{Mass of drug in microspheres}}{\text{Mass of microspheres}} \times 100 \quad (2)$$

The morphology of microsphere composites was characterized using FESEM (NovaNanoSEM450, FEI, USA). Frozen dried microspheres were sputter-coated with gold–palladium and observed under FESEM. Meanwhile, the antimicrobial activity was assessed by the agar well diffusion method. Various amounts of powdered microspheres (25, 50, 75, and 100 mg) were dissolved in 1 ml of distilled water, respectively. Microbes were seeded on solid agar and incubated at 37 °C for 24 h. In brief, inocula of 10^5 CFU/ml were obtained by dilution of microbial liquid cultures with sterile Mueller Hinton broth (MHB), and MHA was then swabbed (sterile cotton swabs) with the microbial suspensions prepared from 24-h-old broth cultures. This was followed by creating agar wells using a sterile borer. Then, about 200 µl of microsphere solutions with diverse concentrations were added to the wells before incubation at 37 °C for 24 h. Drug-free PVAMS were used as a negative control. Then the diameter of the inhibition zones (mm), if any, was evaluated. Experiments were repeated three times.

2.4 Preparation of silk sericin

Bombyx mori cocoons were sliced into small pieces, and SS was obtained using a high temperature and pressure degumming technique [38]. In brief, cocoons were placed in distilled water (10 g in 300 mL) and autoclaved at 120 °C for 1 h. After filtration through filter paper followed by centrifugation to eliminate silk fibroin, the SS solution was concentrated to the preferred concentration by dialysis against PEG solution and lyophilized. The SS powder was kept at -20 °C until use. The SS extraction procedure is summarized in Fig. 1B.

2.5 Preparation of microsphere hydrogels

Poly (vinyl alcohol) was added to deionized water and stirred constantly at 90 °C for 4 h to constitute a 2% uniform solution (Fig. 1C). The SS solution (2%) was prepared by dissolving the necessary amount of SS in distilled water with gentle shaking at 90 °C for 1 h. A volume of SS (0.4 mL) solution was blended with PVA solution (0.6 mL) to prepare a PVA/SS solution. Next, 100 mg of each PVAMS were mixed in 1 mL of PVA/SS solution and the mixture was filled into a 1 mL syringe (BD 5 mL Syringe Precision Glide Needle 20G). Freeze–thaw cycles (8 h at -20 °C and 4 h at RT for two cycles) were applied to the suspension to form a physically crosslinked PVA/SS hydrogel with embedded PVAMSs. The physically crosslinked composites including drug-free poly (vinyl alcohol) microsphere@Poly (vinyl alcohol) /silk sericin hydrogel (drug-free PVAMS@PVA/SS hydrogel), gentamicin-poly (vinyl alcohol) microsphere@Poly (vinyl alcohol) /silk sericin hydrogel (GEN-PVAMS@PVA/SS hydrogel), vancomycin-poly (vinyl alcohol) microsphere@Poly (vinyl alcohol)/silk sericin hydrogel (VA-PVAMS@PVA/SS hydrogel), and vancomycin/gentamicin-poly (vinyl alcohol) microsphere@Poly (vinyl alcohol)/silk sericin hydrogels (VG-PVAMS@PVA/SS hydrogel) were subsequently removed from the syringes and kept at 4 °C for further use. The procedure is summarized in Fig. 1.

2.6 Analytical methods and characterization techniques of microsphere hydrogels

2.6.1 Field emission scanning electron microscopy (FESEM)

The cross-sectional investigations of the produced microsphere hydrogel composites were carried out by FESEM (Nova33NanoSEM450, FEI, USA). All frozen-dried samples were sputter-coated with gold palladium and then observed under a microscope.

2.6.2 Fourier transform infrared (FTIR)

The physicochemical characterization of the produced microsphere hydrogel composites was performed with FTIR (VERTEX 70, Bruker, Germany). The sample preparation and measurements were processed as described above for microspheres.

2.6.3 X-ray diffraction (XRD)

An X-ray diffractometer (X'Pert3 Powder, PANalytical B.V, Netherlands) equipped with Cu Kα radiation (λ = 1.54 Å) at 40 kV and 40 mA was used to examine the crystalline structure of produced microsphere hydrogel composites. The angle of continuous scanning varied from 10 to 70°. The infrared spectra were processed by software to evaluate the results.

2.6.4 Thermogravimetric analysis (TGA)

The thermal performance of samples was assessed with TGA (TGA8000, PerkinElmer, USA) under a nitrogen atmosphere and at a heating rate of 10 °C/min from RT to 600 °C.

2.6.5 Swelling ratio (SR)

Samples were dehydrated at 50 °C in a vacuum oven for 6 h and the sample mass (We) was established. The dried samples were immersed in deionized water, held at 37 °C, and weighed (Ws) at precise time periods. The SR of samples was established using the subsequent Eq. (3).

$$\mathrm{SR}\ (\%) = \frac{W_s - W_e}{W_e} \times 100 \tag{3}$$

2.6.6 Release of SS, VA, and GEN from the hydrogels

The release of SS from hydrogels was obtained after putting the hydrogels into PBS (pH 7.4) at RT with constant stirring in a closed container. The hydrogels (1 mL) were taken out at diverse instant points (0, 1, 15, 30 min, 1, 2, and 3 days), and the quantity of SS in the solution was determined using a BCA protein assay kit. In brief, the solvable SS was collected, blended with BCA reagents, and incubated at RT. The absorbance was established at 562 nm, and the quantity of SS released was compared with a BSA standard curve.

To evaluate the VA and GEN releases, we established a correlation between VA and GEN concentrations and UV-spectrophotometry absorption, respectively. The result showed UV-spectrophotometry absorption was closely correlated with VA and GEN concentrations, indicating it could be used for the purpose of drug release. The release of VA and GEN was tested in PBS (PH 7.4) at 37 °C. At given time points, an aliquot was levied from the solution immersing the different samples to evaluate the VA and GEN release profiles according to their given absorbance (282 for VA and 355 for GEN). All experiments were performed in triplicates. The amount of drug released was calculated using Eq. (4).

$$\mathrm{Release}\ (\%) = \frac{\mathrm{Amount\ of\ drug\ released}}{\mathrm{Total\ drug\ loaded}} \times 100 \tag{4}$$

2.6.7 Rheological properties test

For each hydrogel, 1 mL was used for rheological studies conducted on a controlled stress rheometer (Kinexus ultra + , Malvern Instrument Ltd., U.K.) using a 50 mm parallel plate and a 0.5 mm gap distance at 25 °C. The amplitude sweep strain controlled was performed at a fixed oscillation frequency of 1 Hz and a variable applied shear strain of 1–1000% with samples per decade of 10. For the cyclic strain measurements, the frequency was set at 1 Hz. The hydrogels then underwent testing through a multi-step process, being subjected to 1% strain for 100 s, 100% strain for 100 s, 200% strain for 100 s, and 800% strain for 100 s. A shear rate ramp linear evaluating sample viscosity was performed as well, with a shear rate ranging from 0.1 s^{-1} to 3000 s^{-1}, a ramp time of 2 min, and a sample number of 20 for all tested hydrogels at a constant temperature of about 25 ± 0.1 ºC.

2.6.8 Antimicrobial studies

The disk diffusion method was utilized, with MRSA, *P. aeruginosa,* and *E. coli* as the selected test bacteria. Nutrient agar and nutrient broth were prepared. The microbes were cultured for 24 h at 37 °C in nutrient broth. Successive dilutions were performed to achieve the desired numbers of microbes and test concentrations. Agar plates were then inoculated with 10^5 CFU/mL of bacteria distributed over

the agar surface. Thereafter, hydrogels were incised (1 cm) and placed on the bacterial solid cultures before taking them to incubation at 37 °C for 24 h after which a ruler was used to measure the diameter of the inhibition zones, if any. All steps were carried out aseptically.

2.6.9 Biocompatibility testing

To study the effects of samples on the behavior of skin cells, HaCaT and 3T3 cell lines were used. Cells were maintained in DMEM complemented with 10% FBS and 1% PS at 37 °C and 5% CO_2 in a humidified air incubator. The media was replaced every 2 days. For *in vitro* studies, HaCaT and 3T3 cells from passages 3–6 were used. The samples were sterilized by immersion in 75% (v/v) ethanol for 1 h, followed by rigorous washing with sterile PBS (pH 7.4) three times to remove the alcohol constituents. The sterile scaffolds were incubated in the above complete media at 37 °C with 5% CO_2 to prepare the extracts. After incubation for 24 h, all scaffolds were kindly removed and the extracts were preserved aseptically for further assessment of their cytotoxicity. For the latter purpose, HaCaT and 3T3 cells were seeded at a density of 10^4 cells/cm^2 in 96-well plates with 100 µL of complete media and kept in culture for 24 h to form a semi-confluent monolayer. Then, the culture media were completely substituted with sample extracts, and the cells were then incubated for a further 24 h, 48 h, and 72 h. Regular culture medium was used as a control. At the different time points, cell viability was determined by the CCK-8 assay. Briefly, the CCK-8 solution was added to ongoing cultures with refreshed media at a ratio of 1:10. Cultures were returned to incubation for 1.5 h, after which WST-8 (water-soluble tetrazolium salt contained in the CCK-8 kit) was reduced to formazan (a yellow-colored product), which is soluble in the culture medium by dehydrogenases in viable cells. The absorbance of each tested sample at 450 nm was then measured using a microplate reader (MultiskanEX, Thermo Fisher Scientific, USA). The quantity of the formazan dye produced by the activity of dehydrogenases in cells correlates with the number of viable cells. The experiments were performed in triplicates. Furthermore, the cells cultured with the extracts were double-stained with calcein AM and propidium iodide (live/dead cell stains, respectively) staining. The stained cells were observed under a confocal microscope (FV1000, Olympus, Japan).

2.6.10 Hemolitic test

Three milliliters of rat blood obtained by cardiac puncture (Fig. S6, Supplementary Information) were washed four times with 14 mL of PBS solution by centrifugation at 500 g for 10 min at 4 ºC. Then, the supernatant was removed and the red blood cell (RBC) pellet was resuspended at 2% with PBS. The prepared hydrogels, Triton X-0.5 (positive control), and PBS (negative control) in the amount of 150 µL were added (respectively) to 1350 µL of RBC solution in tubes. Then, different tubes were placed in incubation at 37 °C under shaking (40 rpm) for 6 h. Afterward, the suspensions were put through centrifugation at 2500 g for 5 min. The results were analyzed macroscopically, then 100 µL of the supernatant from each tube was placed into a 96-well plate. The absorbance was read at 540 nm in a microplate reader (MultiskanEX, Thermo Fisher Scientific, USA). The percentage (%) of hemolysis was established as:

$$\text{Hemolysis (\%)} = \frac{(\text{Absorbance}_{\text{sample}} - \text{Absorbance}_{\text{PBS}})}{(\text{Absorbance}_{\text{Tritonx}-0.5} - \text{Absorbance}_{\text{PBS}})} \times 100 \quad (5)$$

2.7 *In vivo* animal experiment

The burn wound healing effectiveness of drug-free PVAMS@PVA/SS hydrogel and VG-PVAMS@PVA/SS hydrogel was studied using male Sprague–Dawley (SD) rats aged 7–8 weeks (200–250 g). All animal experiments were performed with the approval of the Hubei Provincial Center for disease control and prevention. The rats were bred individually in standard cages kept at 24 ± 2 °C with 50–70% humidity and subjected to 12 h of light/dark cycles while having access to food and water ad libitum. All rats were permitted to acclimatize to the laboratory environment for 7 days prior to the experiment. Eighteen rats were anesthetized by intraperitoneal injection of 10% chloral hydrate (300 mg/kg); then dorsal hairs were removed with a clipper before using a razor blade for the entire shaving. After successive sterilization of skin using iodine and 75% ethanol, three full-thickness burn wounds were generated on the dorsal side of each rat with a custom-made aluminum rod, which was heated to 100 ºC over an open flame for 15 s. The deep burn wounds affecting the three skin layers were histologically confirmed at days 0, 1, and 2 post-rat burning without treatment. For dressing testing, the burn wounds of each test animal were treated with commercially available Tegaderm™ film as a control, drug-free PVAMS@PVA/SS hydrogel, and VG-PVAMS@PVA/SS hydrogel, respectively. All dressings were changed every two days during all the experiments. At each dressing change, the burn wound was debrided if necessary, especially after the first 48 h, and gently cleaned with sterilized saline. Before further examinations, the wound appearance for individual wounds was photographed on days 0, 2, 5, 7, 10, 14, and 21. The burn wound area was then measured by ImageJ (NIH, USA) to calculate the wound healing rate following the Eq. (6):

$$\text{WHR} = \frac{Ai - \text{Af}}{Ai} \quad (6)$$

where WHR is the wound healing rate, A_i and A_f represent the burn wound area at day 0 and day n, respectively.

Next, microbiological analyses of burned skin were evaluated on days 3, 7, 14, and 21. Bacterial counts on burn wound beds were performed using the moist swab technique.

2.7.1 Histopathological and immunological analyses

The rats were sacrificed at different experimental endpoints (days 7, 14, and 21) and their tissues were extracted, washed with normal saline, fixed with 4% paraformaldehyde solution, embedded in paraffin, sectioned, dewaxed with a series of xylene and ethanol, and stained with hematoxylin and eosin (H&E) or Masson's trichrome reagents (Wuhan Servicebio Technology CO., LTD) for histopathological analysis.

Immunohistochemistry analysis was accomplished by first slicing paraffin-infiltrated tissue with a microtome and then mounting the section onto charged slides. The sections were dewaxed with serial xylene, ethanol, and washed with distilled water. Then the tissue sections were processed for antigen retrieval, followed by blocking endogenous peroxidase activity. The treated tissue sections were incubated with 3% BSA for 30 min at RT to avoid non-specific binding, followed by incubation with primary antibodies (diluted with PBS) overnight at 4˚C in a humidity chamber to prevent evaporation of the antibody solution.

The used primary antibodies from Wuhan Servicebio Technology CO., LTD were anti-CD31 (CD31, GB113151, dilution 1:500), anti-CK14 (CK14, GB11803, dilution 1:1000), and anti- α -SMA (α-SMA, GB111364, dilution 1:200). Then, the tissues were incubated with a secondary antibody (HRP-labelled goat anti-rabbit, GB23303, dilution 1:200) for 50 min at RT. Finally, the DAB (diaminobenzidine) substrate of HRP was used for chromogenic staining, followed by dehydration sealing with alcohol, xylene, and neutral gum. Observation was done under a microscope (XSP-C204, CIC, Germany).

By immunofluorescence, myeloperoxidase (MPO) and malondialdehyde (MDA) assays were also carried out. After tissue dewaxing, antigen retrieval, and successive incubations with BSA, primary antibodies from Wuhan Servicebio Technology CO., LTD (anti-MPO, GB11224, dilution 1:500; anti-MDA, GB111891, 1:200) and secondary antibodies (CY3 goat anti-rabbit, GB21303, dilution 1:300, Servicebio), the DAPI was used to counterstain the samples for 10 min at RT in the dark, followed by slice stamping with an anti-fluorescence quench seal before collection of images under a fluorescence microscope (Nikon Eclipse C1, USA).

2.8 Statistical analysis

For means comparison among groups, one-way analysis of variance (ANOVA) was used with Tukey's multiple comparison test for the post-hoc pairwise comparisons, in Origin Pro 8 software. All experiments were done in triplicates. Statistical significance level was set at $P < 0.05$ with NS indicating no significance, *indicating $P < 0.05$, ** indicating $P < 0.01$, and *** indicating $P < 0.001$.

3 Results and discussion

3.1 Physical and chemical properties of vancomycin and gentamicin

VA and GEN sulfate were chosen for the fabrication of our drug-loaded injectable microspheres hydrogel because they have antimicrobial potential against both Gram-positive and Gram-negative bacteria, particularly strains of MRSA and VISA for VA, and for GEN, Streptococcus, Proteus, MDR Pseudomonas, and Staphylococcus (including strains resistant to colistin, tetracycline, kanamycin, and chloramphenicol) [34–37]. The drugs were identified by confirming their known physical and chemical properties. Moreover, the ninhydrin test revealed the presence of primary or secondary amine groups able to crosslink with SS and PVA and form a stable microsphere hydrogel (Table S1 and Fig. S1, Supplementary Information).

3.2 *In vitro* interaction between vancomycin and gentamicin

The continuous increase in the occurrence of antimicrobial resistance has jeopardized the effective treatment of infections related to burn wounds, emphasizing the necessity for substitute therapies. Drug combination, such as that of VA and GEN in the present study, is a potential alternative. To study the potential interaction between VA and GEN for the different strains considered herein, a standard time-kill method was utilized. MICs (Table S2, Supplementary Information) were chosen as test concentrations. Findings from the time-kill analyses are shown in Fig. 2. In Fig. 2A, the time-kill curve showed that GEN reduced the number of colonies of MRSA from 7log10 CFU/mL to 5.9log10 CFU/mL after 9 h of incubation, which then increased to 8log10 CFU/ml after 24 h of incubation, remaining significantly lower than the bacteria number in the control (8log10 CFU/mL). This low killing efficiency can be justified by the fact that the concentration used was the MIC and not the MBC. What is more, GEN is known not to be the first choice drug for MRSA eradication due to its somewhat poor performance against this species [39]. As for VA, it decreased the number of colonies of MRSA from 7 log10 CFU/mL to 4 log10 CFU/mL after 24 h of incubation, thanks to the high specificity of its action against Gram-positive bacteria such as MRSA [34]. The combination of VA and GEN reduced

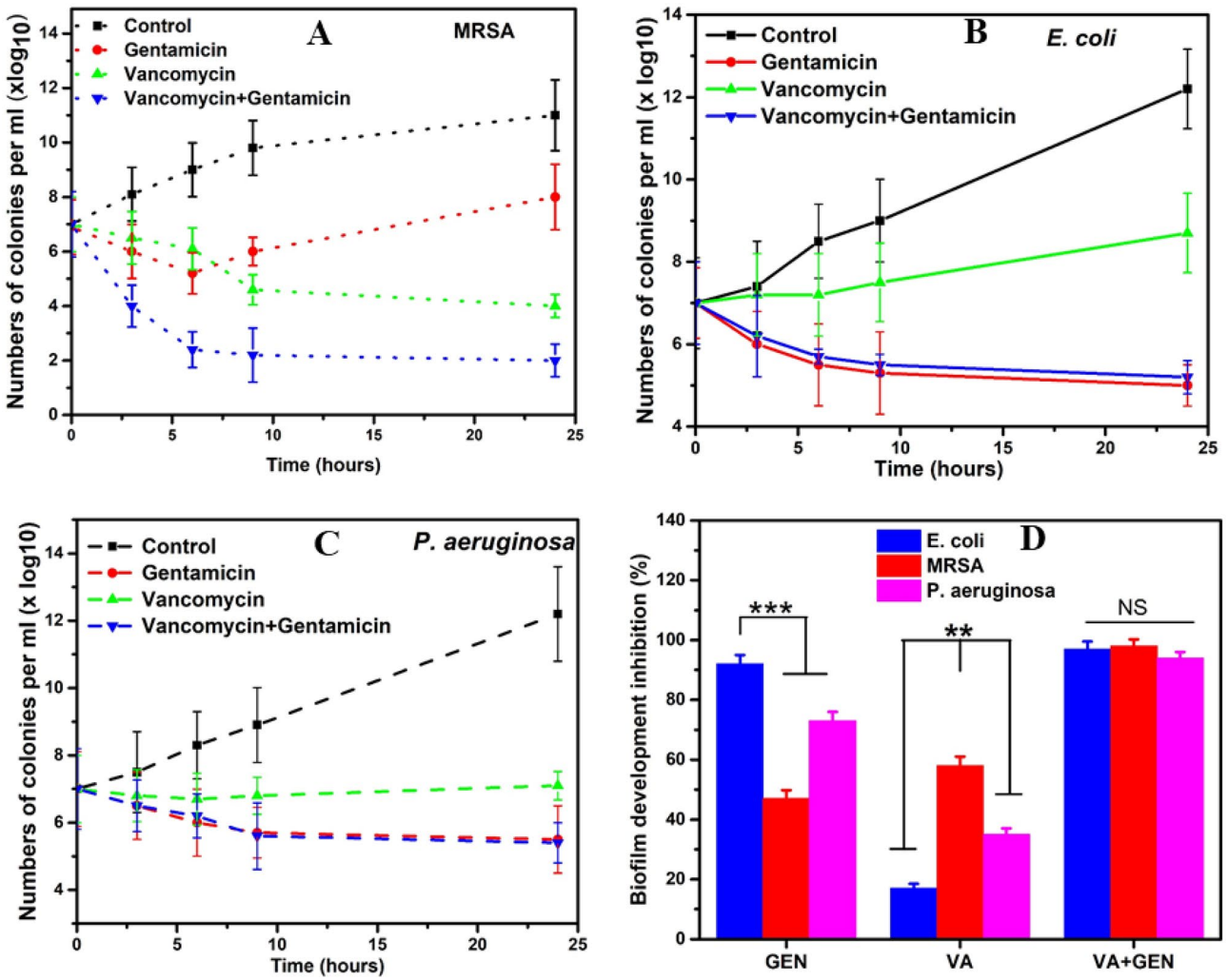

Fig. 2 Killing rates induced by gentamicin (GEN), vancomycin (VA), and gentamicin + vancomycin (VA + GEN) over 24 h. (**A**) MRSA, (**B**) *E. coli* (**C**), *P. aeruginosa,* and (**D**) Antibiofilm activity of VA, GEN, and VA + GEN. N = 3 per group. NS: no significance, *P < 0.05, **P < 0. 01, *** P < 0.001. n = 3 per group

the number of MRSA colonies from 7 log10 CFU/mL down to 2 log10 CFU/mL (Fig. 2A). In Fig. 2B, the time-kill curve showed that GEN reduced the number of *E. coli* colonies from 7 log10 CFU/mL to 5 log10 CFU/mL. In the presence of VA, however, *E. coli* kept growing, although slower than the control, with numbers increasing from 7 log10 CFU/mL to 8.3 log10 CFU/mL after 24 h of incubation, confirming the inefficiency, with a few exceptions, of this drug against Gram-negative bacteria such as *E. coli.* In fact, the resistance of Gram-negative bacteria to VA is explained by the large molecular size (1200–1600 Da) of the drug, which prevents its penetration into the bacterial cell through the porin proteins of its complex outer membrane. Indeed, only hydrophilic molecules that are less than 600 Da are allowed through porins by passive diffusion [40]. Hence, the action spectrum of VA is limited to Gram-positive germs. When it was combined with GEN, however, the number of *E. coli* colonies could be reduced from 7 log10 CFU/mL to 5.2 log10 CFU/mL.

In Fig. 2C, the curve illustrates the decrease in the number of colonies of *P. aeruginosa* as GEN was used, from 7 to 5.6 log10 CFU/mL. In the presence of VA, the number of *P. aeruginosa* colonies reduced from 7 log10 CFU/mL to 6.8 log10 CFU/ml after 9 h of incubation, before starting to increase to 7.1 log10 CFU/mL after 24 h. The drug combination (VA + GEN) then helped reduce the number of colonies from 7 log10 CFU/mL to 5.4 log10 CFU/mL. Overall, the results of the time-kill experiment demonstrated that VA can act synergistically with GEN against MRSA more strongly than against *P. aeruginosa*, probably by increasing the intracellular penetration of GEN. For Gram-positive bacteria such as MRSA, VA acts on peptidoglycans, thus altering membrane permeability, which is probably a natural barrier to GEN; this would allow

the GEN to penetrate in higher quantities in the bacteria (Fig. 7K-L). Antibiotics with a high molecular weight, such as VA, can use several strategies to affect Gram-negative bacteria. Thus, they can presumably diffuse passively through the outer membrane or be uptaken by the cells independently of the porins (Fig. 7L). Furthermore, the positively charged hydrophilic molecules can interact electrostatically with the negatively charged phosphate groups of lipid A and thus destabilize the structure of lipopolysaccharide and then facilitate the penetration of VA into the periplasm [29]. Once in the periplasm, it can diffuse through the inner membrane or be inadvertently taken up by membrane transporters [41]. This explains why the VA inhibits RNA synthesis in some strains of *P. aeruginosa* sensitive to the drug [42], which is reflected as growth inhibition in our findings. The same trends in the results of VA association with Trimethoprim and Nitrofurantoin against Gram-negative bacteria were reported by Zhou et al. [43]. Thus, this study confirms the findings of enhanced activity of the VA + GEN association against MRSA. The low enhanced activity of this drug combination was found against *P. aeruginosa,* and no synergistic effect against *E. coli* was highlighted. The drug combination (VA + GEN) holds the advantage of having a broader spectrum of antimicrobial activity against microorganisms involved in burn wound infections than a single drug.

3.3 Antibiofilm inhibition

Biofilms are composite populations of surface-attached collectives of pathogens fixed in a self-secreted extracellular polysaccharide matrix [44]. The biofilm operates as a solid barrier to antimicrobials and the immune system, making microbes more resistant to conventional drugs and disinfectants [44]. Typical antimicrobials and disinfectants frequently fail to eliminate infections because they do not penetrate biofilms completely to reach the hidden microbes or are unable to harm microbes of all species and metabolic states in the films [44]. The potential of VA, GEN, and (VA + GEN) against biofilm development from isolated *E. coli, P. aeruginosa,* and MRSA was investigated using crystal violet staining (Fig. 2D). In the biofilm inhibition assay, drug combinations yielded the highest inhibition rates of 97 ± 2.5% for *E. coli*, 94 ± 2% for *P. aeruginosa*, and 98 ± 2.2% for MRSA. VA led to 58 ± 3% inhibition for MRSA, 35 ± 2% for *P. aeruginosa*, and 17 ± 1.5% for *E. coli*. With GEN, 92 ± 3% biofilm inhibition was obtained for *E. coli*, 47 ± 2.8% for MRSA, and 73 ± 3% for *P. aeruginosa*. In sum, it appears that with the drug combination, a synergistic inhibitory effect was obtained against the studied microorganism, namely MRSA, in terms of biofilm development.

3.4 Characterization of PVA microspheres

Four types of microspheres were prepared, including drug-free PVAMS, GEN-PVAMS, VA-PVAMS, and VG-PVAMS. The microspheres were characterized by examination of their FTIR and XRD spectra, drug encapsulation efficiency, morphology, antimicrobial activity, and biocompatibility. The infrared (IR) spectra (Fig. 3A) of drug-free PVAMS showed the feature peaks of PVA at 3261 cm^{-1} (O–H stretching), 2929 cm^{-1} (C-H stretching), 1718 cm^{-1} (-CO stretching), and 1470 cm^{-1} (CH_2 deformation) [45, 46]. GEN sulfate exhibited its characteristic absorption peaks of amide I at 1653 cm^{-1}, amide II at 1535 cm^{-1} and O–H stretching at 3408 cm^{-1}. The FTIR spectra of GEN-PVAMS contains bands characterizing both individual components, suggesting their successful and optimal blending, but the amide I shifted from 1653 cm^{-1} to 1644 cm^{-1}, whereas the amide II decreased in intensity and the O–H stretching shifted from 3349 to 3399 cm^{-1}, indicating that GEN slightly modified the inherently ordered structure of PVA in microspheres. In the spectrum of VA-PVAMS, characteristic peaks were observed at 3392 cm^{-1} (stretching vibration of N–H), 1652 cm^{-1} (stretching vibration of C-H and C-N), 1503 cm^{-1} (bending vibration of N–H and C = O), 1064 cm^{-1} (stretching vibration of C-O) and 1021 cm^{-1} (stretching vibration of C-N). The absorption bands in VA-PVAMS at 3398 cm^{-1}, 1644 cm^{-1}, and 1054 cm^{-1} then confirmed the presence of VA in PVAMS. VG-PVAMS exhibited the characteristic bands of all components at 3370 cm^{-1}, 2922 cm^{-1}, 1713 cm^{-1},1643 cm^{-1} and 1433 cm^{-1}.

The XRD (Fig. 3B) of PVA powder showed a strong diffraction peak at 19.4°, equivalent to its crystal planes [47]. Due to their amorphous nature, the GEN and VA powders did not show any crystalline peak. Compared to PVA powder, the strong diffraction peak characteristic of PVA remained but decreased in intensity and shifted at 18° in the drug-free PVAMS as in the drug- PVAMS, suggesting the addition of drugs and the microsphere fabrication process did not affect the crystallinity of PVA. Microsphere morphology was evaluated using FESEM (Fig. 4A-H) and optical microscopy (Fig. S3, Supplementary Information). All microsphere formulations produced spherically shaped particles (Figs. S2 and S3, Supplementary Information) with an average size diameter and standard deviation of 31.41 ± 6.04 µm for drug-free PVAMS (Fig. 4I), 29.11 ± 4.27 µm for GEN-PVAMS (Fig. 4J), 32.78 ± 5.64 µm for VA-PVAMS (Fig. 4K), and 29.53 ± 3.31 µm for VG-PVAMS (Fig. 4L), within the acceptable values of polydispersity index (≤ 0.2) (Fig. 4E-H) [48] and choice of adequate size diameter (< 50 µm) for parenteral injection [49].

The results of the analysis of encapsulation efficiency and drug loading capacity are shown in Table 1. The encapsulation efficiency (EE) was studied by UV/visible

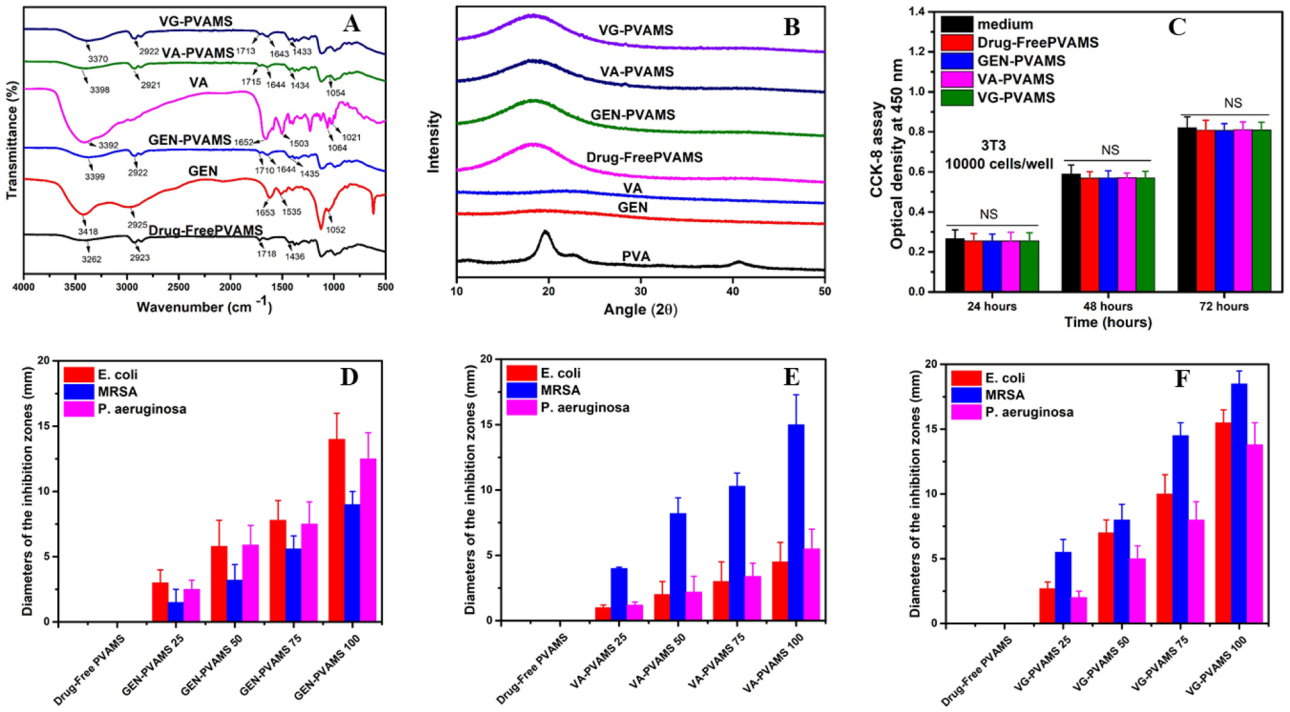

Fig. 3 Characterization of drug-free PVAMS, GEN-PVAMS, VA-PVAMS, and VG-PVAMS. (**A**) FTIR spectra, (**B**) XRD spectra, (**C**) *In vitro* biocompatibility of microspheres at 100 mg/ml as concentration: viability of fibroblasts cultured in sample extract. Antibacterial activity against *E. coli*, MRSA, and *P. aeruginosa* obtained by the disc diffusion method and expressed as diameters of the inhibition zones (mm) of (**D**) GEN-PVAMS, (**E**) VA-PVAMS, and (**F**) VA-PVAMS at different concentrations (25, 50, 75, and 100 mg/mL). n = 3 per group, NS: no significance

spectrophotometry and was found to be 68 ± 1.54% and 65 ± 1.7% for GEN-PVAMS and VA-PVAMS, respectively, and no significant difference in EE values was found with VG-PVAMS (Table 1). Subsequently, the drug loading capacity of VA and GEN was calculated and was found to be 8.2 ± 0.31% and 8.7 ± 0.47% for GEN-PVAMS and VA-PVAMS, respectively; reduced drug loading capacity was found for VG-PVAMS (Table 1). These results are consistent with the general assumption that a high drug load suggests that the polymer/drug ratio will be low and that the polymer incorporated will not be sufficient to completely trap the drug, which would result in lower encapsulation efficiency.

For antimicrobial studies, the concentrations of microspheres were controlled at 25 mg/mL, 50 mg/mL, 75 mg/mL, and 100 mg/mL. The antimicrobial activity was directly proportional to the concentration of microspheres, suggesting that 100 mg/mL of microspheres exhibited strong antimicrobial activity (Fig. 3D-F). To analyze the biocompatibility of microspheres at different concentrations (Fig. 3C), NIH-3T3 fibroblast cell lines were used. Sample extracts were obtained by submerging the microspheres in the growth media for 7 days and were applied for cell culture. No significant difference was observed in the cytotoxicity of the different microspheres samples compared to the control, suggesting that all samples were biocompatible and the drug concentration did not affect the cell viability.

3.5 Physical appearance of the injectable microsphere hydrogel and rheological properties

Four types of injectable microsphere-loaded hydrogels were prepared, including drug-free PVAMS@PVA/SS hydrogel, GEN-PVAMS@PVA/SS hydrogel, VA-PVAMS@PVA/SS hydrogel, and VG-PVAMS@PVA/SS hydrogel, using the freeze–thaw method (Fig. S4). Moreover, to study the influence of embedded microspheres, PVA/SS hydrogel without microspheres was used as a control. One hundred mg/mL of microspheres in PVA/SS solution was the concentration (10%) used for each microsphere type to prepare the injectable hydrogel since it presented the best antimicrobial activity among the tested concentrations with no cytotoxicity behavior. The final microsphere concentration in the reconstituted suspension normally does not exceed 20% w/v due to viscosity-related issues in syringeability and injectability [49]. The most suitable concentrations of polymers for forming an injectable hydrogel after optimization were 2% for PVA

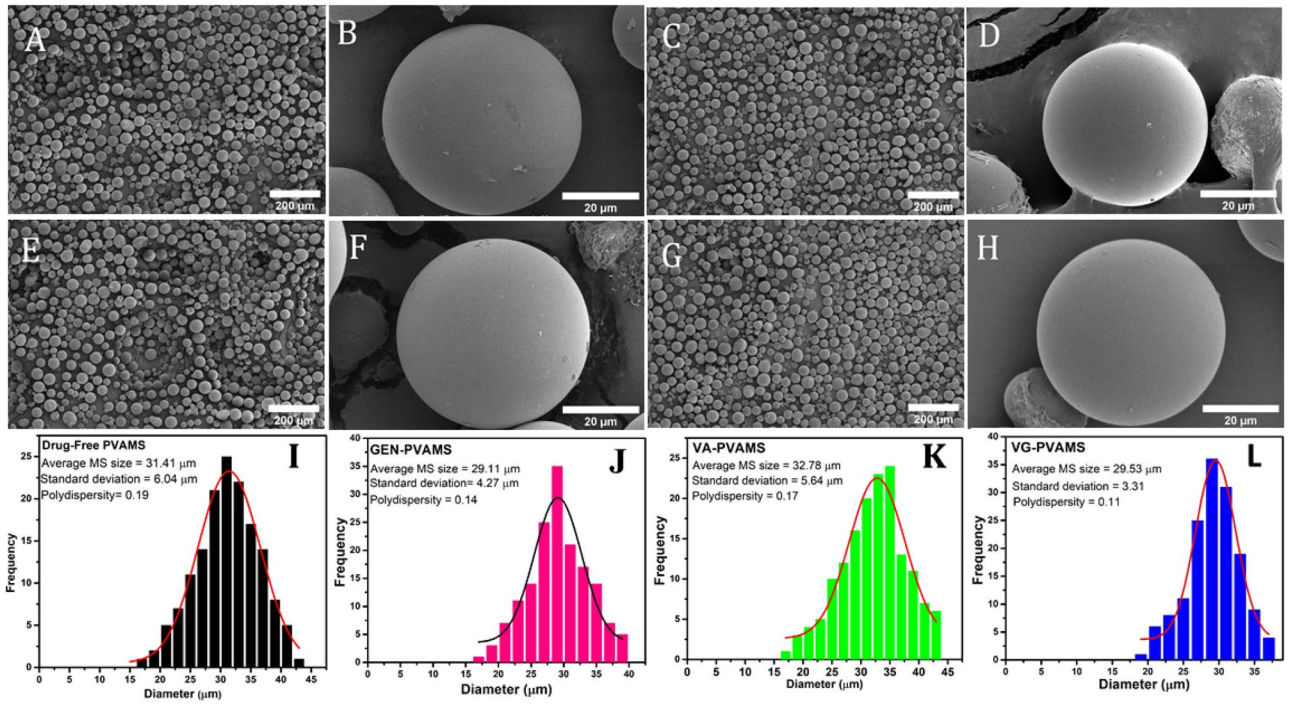

Fig. 4 Morphological characteristics of the microspheres. FESEM micrographs of (**A**-**B**) drug-free PVAMS, (**C**-**D**) GEN-PVAMS, (**E**–**F**) VA-PVAMS, and (**G**-**H**) VG-PVAMS. Magnification 100X (**A**, **C**, **E**, **G**) and 1500X (**B**, **D**, **F**, **H**). Size distribution and polydispersity index (PI) of (**I**) drug-free PVAMS, (**J**) GEN-PVAMS, (**K**) VA-PVAMS, and (**L**) VG-PVAMS. The polydispersity was calculated as the standard deviation divided by the average MS size

and 2% for SS, with a 6:4 as a ratio (data not shown). Such a formulation formed optimal and homogeneous hydrogels after 2 consecutive freeze-thawing cycles. Rheological studies on varied strains were conducted (Fig. 5). For all hydrogels, the elastic modulus (G') predominated over the viscous modulus (G'') in the lower and median strain range, indicating the linear viscoelastic region (Fig. 5A). Hence, the microsphere-loaded hydrogels remained longer in the linear viscoelastic domain. However, the increase in strain over 100% was directly proportional to the predominance of the viscous modulus (G"), leading to the intersection between G′ and G" (G' = G"), which indicates the sol–gel transition or gel point [50]. Thus, overall, high critical strain values were required before the rheograms showed nonlinear responses indicative of a structural breakdown of the hydrogels. This is because of the homogeneous entanglement of the different polymer chains within the materials, reinforcing the hydrogels' networks and enhancing their resistance to deformation before their transition to liquid form (G'' > G').

Table 1 Encapsulation efficiency and drug loading capacity of microspheres

Microspheres	Encapsulation efficiency (mean ± SD) (%)		Drug loading capacity (mean ± SD) (%)	
	Gentamicin	Vancomycin	Gentamicin	Vancomycin
PVAMS	0	0	0	0
GEN-PVAMS	68 ± 1.54	0	8.7 ± 0.47	0
VA-PVAMS	0	65 ± 1.7	0	8.2 ± 0.38
VG-PVAMS	63 ± 2.01	66 ± 1.49	3.52 ± 0.24	3.94 ± 0.28

The loss tangent (tan delta = G "/G') was calculated for all tested hydrogels (Fig. 5B). For all hydrogels, the G′ was significantly greater than the G″ at the start of strain oscillation up to the critical value, resulting in lower values (< 1) of tan δ. The tan δ values of the VG-PVAMS@PVA/SS hydrogel before the gel point (tan δ = 1) were the lowest among all tested samples, illustrating the predominant elastic (as opposed to viscous) nature of the hydrogel. Hence, the smaller the tan δ, i.e., much lower than 1, the better suited the VG-PVAMS@PVA/SS hydrogel is for deeper injection. The viscosity of the gels declined with a rising shear rate, revealing their shear thinning behavior, which would facilitate extrusion-based injection processes (Fig. 5C). From a lower shear rate up to $\gamma \approx 750\ s^{-1}$, the hydrogels without microspheres (PVA/SS hydrogel) had a higher viscosity than those with microspheres, in accordance with other studies that showed that microspheres decrease hydrogel viscosity

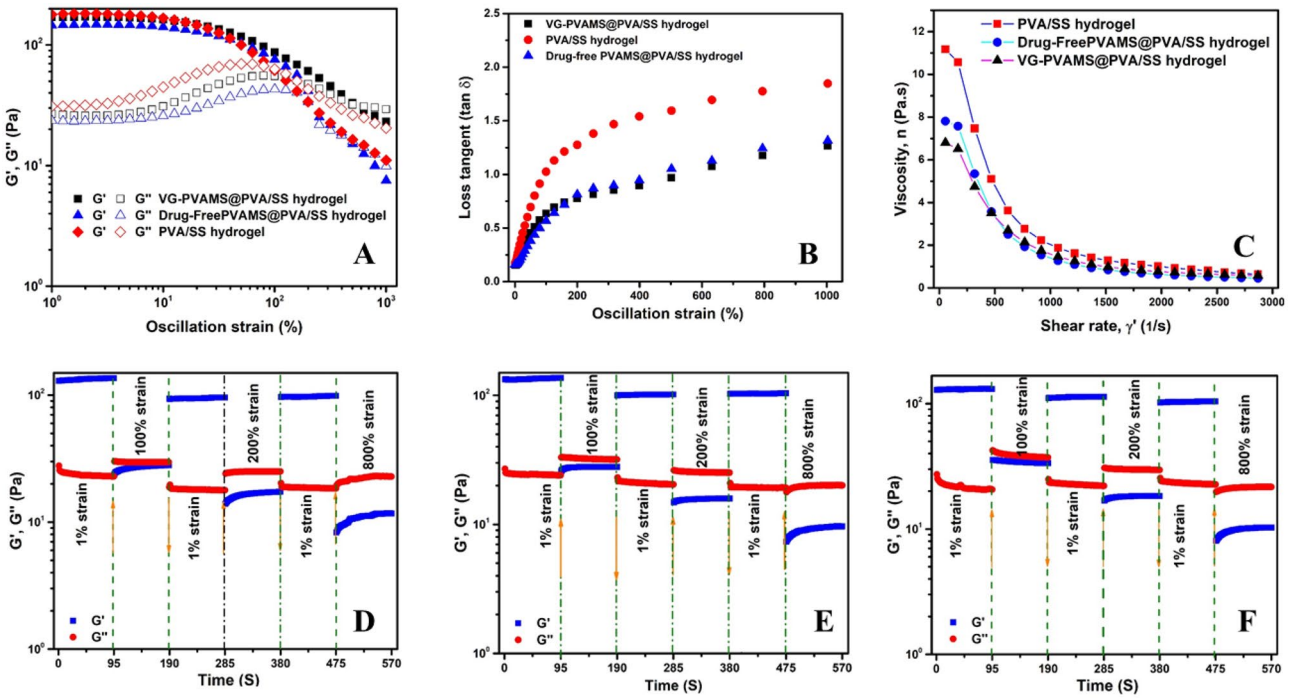

Fig. 5 Rheological properties of the hydrogels. (**A**) Strain sweep, (**B**) loss tangent, and (**C**) Viscosity measurements of hydrogels. Alternate strain sweep at 1 Hz of (**D**) PVA/SS hydrogel, (**E**) drug-free PVAMS@PVA/SS hydrogel, and (**F**) VG- PVAMS@PVA/SS hydrogel

[51]. What is more, the hydrogels with drug-loaded microspheres exhibited lower viscosity than those with drug-free microspheres, suggesting that the drugs (VA + GEN) also decreased the viscosity slightly at a lower shear rate up to $\gamma \approx 250\ s^{-1}$. However, at higher shear rates, the viscosity of all hydrogels remains nearly constant ($\gamma > 1000\ s^{-1}$) due to polymer chain alignment in the direction of gel flow.

The recoverability behaviors of the samples under high strains were assessed by alternate strain sweep (Fig. 5D-F). It was observed that before application of high shear strain, the drug-free PVAMS@PVA/SS hydrogel (Fig. 5E) and VG-PVAMS@PVA/SS hydrogel (Fig. 5F) held G′ at ≈145 Pa and G' at ~150 Pa; at high shear strain, it appeared the networks within these gels were impeded, with G' dropping to ~ 32 Pa and G'' ≈ 36 Pa at 200% strain (9 Pa and 10 Pa at 800% strain, respectively) (Fig. 5E-F). When the high shear strain was discontinued and replaced by a low shear strain (1%), the gels recovered more than 90% within seconds, suggesting that the microspheres did not affect the recoverability of hydrogels after the discontinuation of high shear compared to PVA/SS hydrogel (Fig. 5D).

Hydrogel syringeability and injectability through a narrow 20 G needle were further tested (Fig. S3, Supplementary Information). Syringeability, defined as the capability of the hydrogel to pass across a hypodermic needle from the bowl of the syringe, was determined by the ease of gel removal and the absence of clogging. Increased viscosity, concentration and solid size (microspheres) all adversely affect the syringeability [52]. The hydrogel used in this study was more elastic than viscous, and the polymer concentrations used were syringeable; in fact, the average microsphere diameter ranged from 26.22 to 32.42 μm, as required for parenteral injection and drug delivery systems [49]. Commonly, small microsphere size (≤ 3 μm) improves syringeability and necessitates a reduced needle diameter, up to a certain limit under which the microspheres are more disposed to phagocytosis [53, 54]. Therefore, it is essential to balance reducing needle caliber with preventing phagocytosis when choosing the microsphere size.

Overall, all the above findings indicated that the VG-PVAMS@PVA/SS hydrogel was more elastic than viscous, with a recoverability behavior under oscillatory strain; such attributes render the gel suitable for the deep injection corresponding to full-thickness burn wound treatment.

3.6 Morphology of the hydrogels

All microsphere hydrogels exhibited homogeneous morphology, a porous structure with connected porosity but diverse pore arrangements (Fig. 6A-D). Porosity is a very significant parameter for the application of hydrogels in burn wound healing, with highly porous hydrogels resembling the native extracellular matrix (ECM). During application, cells should be able to attach and migrate inside the hydrogel, which

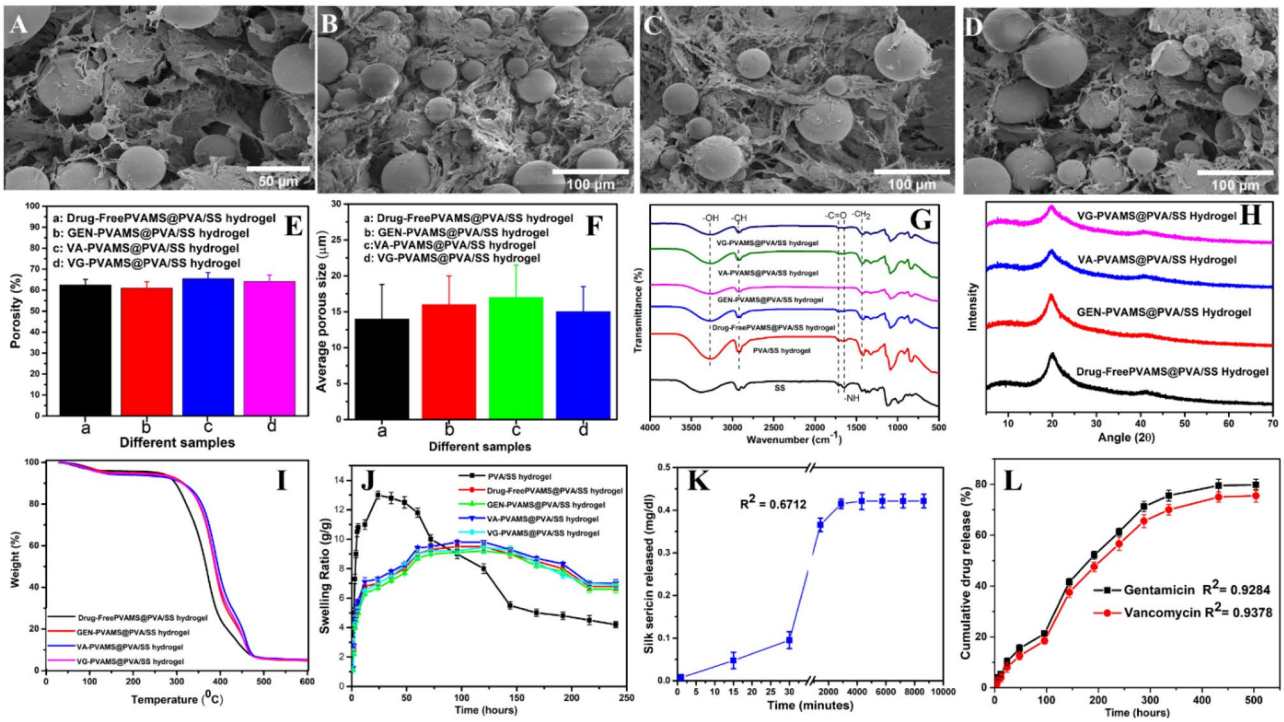

Fig. 6 Characterization of microsphere hydrogels. FESEM micrographs of (**A**) drug-free PVAMS@PVA/SS hydrogel, (**B**) GEN-PVAMS@PVA/SS hydrogel, (**C**) VA-PVAMS@PVA/SS hydrogel, and (**D**) VG-PVAMS@PVA/SS hydrogel. (**E**) Porosity, (**F**) pore size, (**G**) FT-IR spectra, (**H**) XRD spectra, (**I**) TGA curves, (**J**) swelling behavior of different hydrogels. The release profile of (**K**) silk sericin, (**L**) vancomycin and gentamicin from VG-PVAMS@PVA/SS hydrogel. N = 3 per group

requires high porosity. Furthermore, porous structures facilitate gas interchangeability and simple intake of burn wound exudates, both of which are necessary for cell growth and tissue regeneration. Porous structures also allow access of nutrients to cells and cellular products out of cells, provide a suitable environment for cell growth, proliferation, and survival and serve as a microhabitat for moisture holding, preservation, and release of biomolecules [55]. Mainly, the favored porosity should be in the choice of 60–90% [55]. Herein, the porosity was evaluated by the liquid displacement method, and the results are shown in Fig. 6E. The porosities of all prepared injectable hydrogels were more than 60% (Fig. 6E), with a pore size (14–22 μm) (Fig. 6F) that meets the requirements for tissue regeneration (optimal pore size for skin: 20–125 μm) and wound healing [56].

3.7 Physicochemical properties

The FTIR spectra of SS exhibit characteristic peaks such as amide I (C = O at 1630 cm^{-1}), amide II (N–H at 1515 cm^{-1}), and amide III (C-N at 1242 cm^{-1}) [38] (Fig. 6G). The PVA/SS hydrogel exhibits the characteristic peaks of SS and PVA (-OH and -CO stretching), suggesting a successful blending between SS and PVA, but the amide I shifted from 1630 cm^{-1} to 1645 cm^{-1} and the amide II from 1515 cm^{-1} to 1530 cm^{-1}. All microsphere-loaded hydrogels exhibited the feature peaks of all components, suggesting a successful blending between PVA, SS, and drugs (Fig. 6G). XRD spectra were recorded to describe the crystalline structure of the preparations (Fig. 6H). The drugs (GEN and VA) appear not to alter the diffraction peak of PVA, suggesting that the crystallinity was maintained.

Heating at a high temperature is necessary for the sterilization of biomaterials for use in biomedical applications. Furthermore, for wound dressing application in burn patients who frequently develop hyperthermia owing to the prolonged inflammatory phase and given the variation in body temperature, wound dressings should be thermally stable [57]. The TGA spectra of microsphere hydrogels are shown in Fig. 6I. TGA curves illustrated the proportion of the lost weight of the hydrogels upon heating from RT to 600 °C. The initial weight loss from RT to about 300 °C refers to the removal of the remaining water trapped in the hydrogel networks. At the initial weight loss, VA-PVAMS@PVA/SS offered the maximum water loss, followed by VG-PVAMS@PVA/SS, GEN-PVAMS@PVA/SS, and drug-free PVAMS@PVA/SS hydrogel, demonstrating its higher aptitude to captivate moisture from the ambient environment. In burn wound dressing treatments, this would restrain the dehydrating of burn wounds, indicating that VG-PVAMS@PVA/

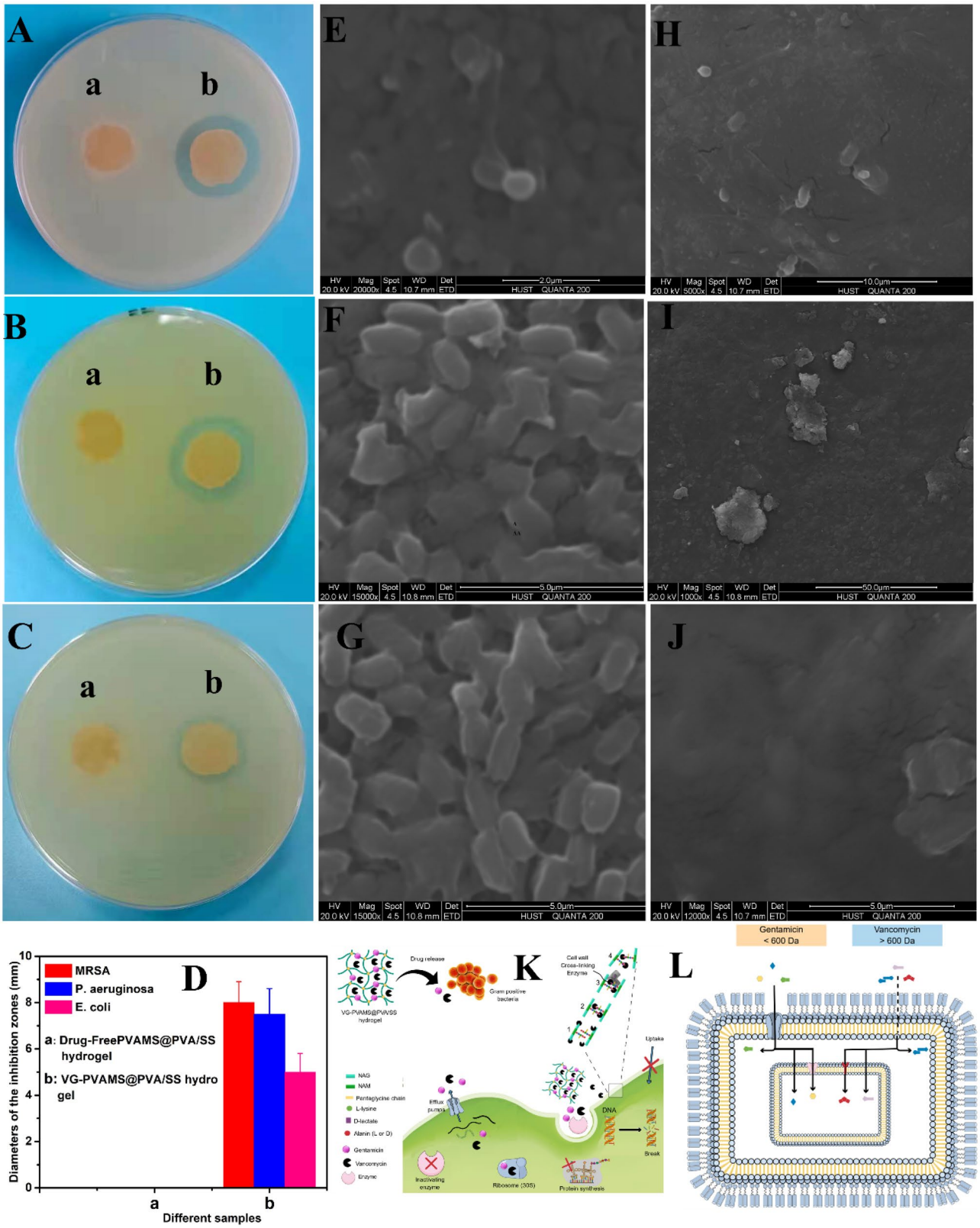

Fig. 7 Antimicrobial activity evaluation of microsphere hydrogels. Disk diffusion method for (**a**) drug-free PVAMS@PVA/SS hydrogel and (**b**) VG-PVAMS@PVA/SS hydrogel against (**A**) MRSA, (**B**) *P. aeruginosa*, and *E. coli* (**C**), and their diameters of the inhibition zones (**D**). Structure of the biofilm formed on agar (**E**) MRSA, (**F**) *P. aeruginosa,* and (**G**) *E. coli.* Biofilms of (**H**) MRSA, (**I**) *P. aeruginosa,* and (**J**) *E. coli* treated with VG-PVAMS@PVA/SS hydrogel. Schematic illustration of the antibacterial mechanism of vancomycin and gentamicin against (K) Gram-positive bacteria and (L) Gram-negative bacteria

SS hydrogel can preserve a moist setting over burn wounds, avoiding dehydration scab development. The second most important thermal degradation took place in the temperature range of 300–480 °C due to the de-polymerization of chain components and decomposition of hydrogel networks. The presence of drugs in the network positively affected thermal stability.

3.8 Dynamic swelling behavior and degradation rate of hydrogels

A chronic wound such as deep burn wounds usually fails to heal because of the production of high amounts of exudates, which can induce maceration of the tissues surrounding the burn wound. Therefore, the injectable hydrogels were analyzed for their aptitude to absorb burn wound exudates through monitoring of their swelling behavior. We examined the swelling property in deionized water compared to the PVA/SS hydrogel without microspheres (Fig. 6J). Material swelling ratio (SR) shows its capacity to absorb water, which is indispensable because it influences numerous features of the hydrogel, such as the diffusion of loaded drugs and cell bioactivity [58]. The PVA/SS hydrogel without microspheres displayed higher water uptake within the first 24 h compared to those with microspheres. After this initial water uptake on the first day, the hydrogel without microspheres decreased its water uptake after ten days due to the decrease in weight. PVA-based hydrogels have been applied as biomaterials; thus, the short period swelling feature of PVA hydrogels has been systematically studied [59]. They typically reach their maximum swelling in one hour, similar to the findings described here for the PVA/SS hydrogel [60]. The hydrogel with microspheres continued to absorb water after day 1 and reached a maximum after 5 days before decreasing during the rest of the testing period. The VA-PVAMS@PVA/SS hydrogel exhibited a higher swelling ratio than that with GEN owing to the large number of hydrophilic hydroxyl groups in VA, which also increased the SR in the VG-PVAMS@PVA/SS hydrogel compared to GEN alone. The long-term swelling behavior of the VG-PVAMS@PVA/SS hydrogel has not been previously described. Our study shows that, contrary to the unloaded gels, all microsphere-loaded hydrogels displayed a long-term water uptake, indicating that the microspheres were the determining factors in the long-term water absorption.

To examine the degradation of different hydrogels, they were soaked in PBS (PH 7.4) for different predetermined time points. The incorporation of drug-free PVAMS and drug-PVAMS in PVA/SS hydrogel decreased the degradation rate compared to PVA/SS hydrogel (Fig. S5D, Supplementary Information). Besides, the type of drug did not affect the degradation rate. All microsphere hydrogels showed a degradation rate of about 70% after 7 weeks, suggesting a sustainable release of bioactive molecules while still offering sufficient time for full-thickness burn wound healing.

3.9 *In vitro* release profiles of silk sericin, gentamicin, and vancomycin

To confirm the physical integrity of the microsphere-loaded hydrogels and to predict their performance in a physiological environment, the release profiles of SS, GEN, and VA from the samples were controlled in PBS (pH 7.4) by the BCA protein assay for SS and UV-spectrophotometer for GEN and VA. The results arranged in Fig. 6K showed a burst release of SS from the VG-PVAMS@PVA/SS hydrogel in the first 16 h because of the hydrophilicity of SS. The burst release was followed by a regular release of SS with an equilibrium phase due to reversible hydrogen bonds within the polymeric hydrogels, which disintegrated progressively in aqueous solutions. The concentration of the accumulated released SS increased without linearity during the testing period, with a correlation coefficient of 0.6712 indicating that the hydrogels released SS at a non-constant rate. Therefore, under physiological conditions, the soluble SS could be released from the microsphere-loaded hydrogels and reach the surrounding cells and tissues by diffusion. This would allow SS to exert its beneficial effects on accelerating burn wound healing by inducing cell proliferation and migration.

Silk sericin encloses positive and negative charges, while PVA is neutral and GEN and VA are positively charged. Thus, the electrostatic force between the opposite charges could favor the interactions of GEN and VA microspheres with PVA/SS hydrogels. To investigate the antibiotic release, we established the correlation between VA and GEN by UV-spectrophotometry. The result revealed that optical density was closely correlated with VA and GEN concentration (Fig. S5A-B, Supplementary Information), showing it could be utilized for the establishment of drug release from microsphere hydrogels. To better understand the role of the PVA/SS hydrogel in the release of VA and GEN, the antibiotic release profile was determined from two kinds of systems over 21 days, namely the VG-PVAMS (Fig. S5C, Supplementary Information) and VG-PVAMS@PVA/SS hydrogel systems (Fig. 6J). As examined, the two systems varied in antibiotic release kinetics so that the integration of VG-PVAMS into PVA/SS hydrogel resulted in a zero-order release without bursting (See R^2 values). The accumulated released concentration of the drugs increased linearly with time, with a correlation coefficient of 0.9284 for GEN and 0.9378 for VA. The result indicates that microspheres alone (VG-PVAMS) and microspheres in hydrogel matrix (VG-PVAMS@PVA/SS hydrogel) release GEN and VA at a constant rate. This result could be accredited to the sequential

GEN and VA release from microsphere hydrogel, in which the drugs should first diffuse throughout the microspheres and then throughout the microporous PVA/SS hydrogel.

The incorporation of drug-loaded microspheres into the PVA/SS hydrogel reduced the release of GEN and VA. From the free microspheres, maximum drug release was achieved after 21 days, at 95.3% and 89.59%, respectively. When the microspheres were embedded in PVA/SS hydrogel, however, the maximum amount of drug released within the same period was reduced to 79.8% for GEN and 75.5% for VA. Nevertheless, despite this reduction in drug release, the levels of solubilized drugs remained above the MIC values (> 8 mg/l for GEN, > 2 mg/l for VA), which keeps the released drugs within the active concentrations (Fig. 7A-D). Therefore, the hybrid hydrogel could be used for slower and longer drug delivery, given the long lead times. The analysis revealed continuous drug release and no significant burst effect was observed, demonstrating that the drugs were homogeneously distributed in the PVA matrix and that there was no important quantity of drugs adsorbed onto the surface of the microspheres. The cumulative release percentage did not reach 100%, as some constitutive amount remained bound in the structure of the microspheres, which did not collapse to release their different constituents but kept their original shape until the experiment was concluded (21 days), emphasizing their stability and structural integrity. A model chronic wound dressing should have a prolonged release of antimicrobials to avoid recurrent dressing changes, reducing the risk of overexposure of the wound to microorganisms [30]. Referring to the drug release profile, the prepared microsphere-loaded hydrogels have confirmed their capability of constituting efficient drug reservoirs with controlled drug release, adapted to achieve and maintain optimal levels of therapeutics for burn dressing applications.

3.10 Antimicrobial activity of prepared microsphere hydrogels

For optimal wound healing, it is extremely important to protect wounds against pathogens that could cause extra damage and delay the healing progression, especially when the wound is chronic, large, or when the patient is particularly at risk, such as in full-thickness burns, for example [61]. Considering the reported antimicrobial property of the GEN and VA combination against both Gram-positive and negative bacteria, the prepared VG-PVAMS@PVA/SS hydrogel was assessed for such bioactivities with drug-free PVAMS@PVA/SS hydrogel as a control. By the agar diffusion method, their antimicrobial potency against Gram-negative (*E. coli, P. aeruginosa*) and Gram-positive (MRSA) was examined, respectively. Widely spread in the environment, the selected microbes are responsible for many burn wound infections. The results indicated that the control demonstrates no inhibition on the growth of the studied bacteria; however, VG-PVAMS@PVA/SS hydrogel impaired the growth of cultured tested bacteria as evidenced by the presence of inhibition zones (Fig. 7A-D), suggesting an inhibitory effect due to the presence of GEN and VA. Hence, as demonstrated in the release assays presented in the section above, GEN and VA are released from the VG-PVAMS@PVA/SS hydrogel, which exerts antibacterial effects, including biofilm eradication (Fig. 7H-J) via multiple mechanisms (Fig. 7E-F).

3.11 Cytocompatibility

To analyze the cytocompatibility of the injectable hydrogels, NIH-3T3 fibroblast and HaCaT cells were used. Fibroblasts and keratinocytes play a significant role in wound healing, including the synthesis of extracellular matrix proteins and cytokines, leading to wound closure [62, 63]. Sample extracts were acquired by immersing the injectable hydrogels in the growth media for 7 days and were applied for cell culture. No significant difference was evidenced in the cytotoxicity of the different experimental samples and the control (Fig. 8A, C-D), indicating the biocompatibility of the hydrogels. Actually, the injectable hydrogels containing SS significantly increased the cell viability when compared to the control at days 2 and 3, underlining the bioactive nature of SS and its cell proliferative effect. Interestingly, there was no significant difference in cell viability between the drug-containing hydrogels and those without, suggesting that VA and GEN did not affect cell viability (Fig. 8C-D).

Hemocompatibility tests were also done to assess the hemolysis effect of the materials on RBC. The results observed macroscopically and spectrometrically showed no hemolysis in all the used samples (Fig. 8B and E), supporting the application of the samples as biomaterials for burn wound healing.

3.12 Potential for burn wound healing

The performance in burn wound healing of the drug-free PVAMS-PVA/SS and VG-PVAMS-PVA/SS hydrogels was investigated *in vivo* for the treatment of full-thickness burn wounds in rats, using Tegaderm™ dressing as a control.

3.12.1 Depth of the burn wounds

Burn wounds can be classified into first-degree, second-degree superficial partial-thickness, second-degree deep partial-thickness, third-degree full-thickness, or fourth-degree full-thickness burns [6, 61]. In a first-degree burn, only the epidermis is affected, without blistering. Superficial second-degree and deep partial-thickness burns concern the papillary dermis and reticular dermis, respectively, and are characterized by blisters that appear either immediately or

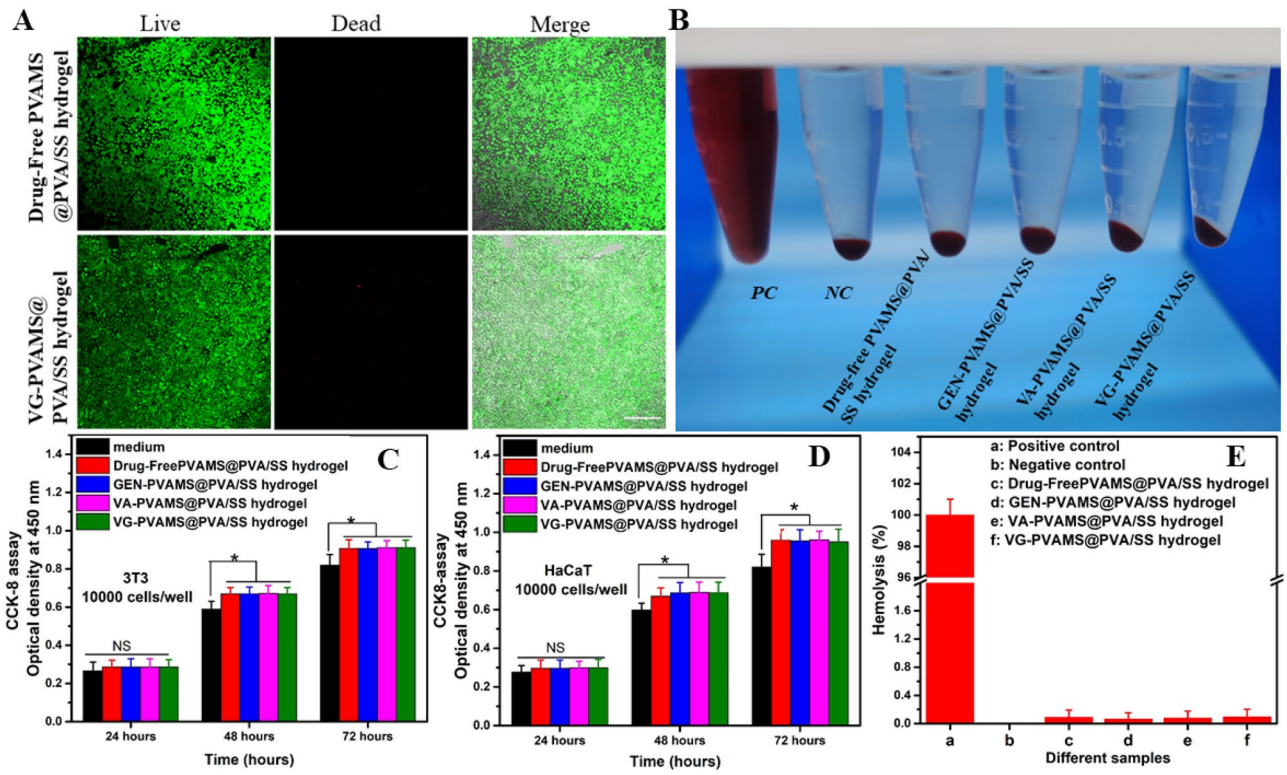

Fig. 8 Biocompatibility of the hydrogels. (**A**) Live/dead fluorescence results of HaCaT cells cultured in drug-free PVAMS@PVA/SS and VG-PVAMS@PVA/SS hydrogels for 3 days. Scale bar 200 μm. (**B**) Photo image of Eppendorf tubes showing the results from hemolysis rate assay of RBC treated with different samples, viability of (**C**) fibroblasts and (**D**) keratinocytes cultured in sample extracts, (**E**) hemolysis rate. NS: no significance, * $P < 0.05$

within hours post-burning [6, 61]. Unlike the superficial second degree, blood vessels and nerve endings are destroyed during the deep partial-thickness burn. In a third-degree burn, the skin is burned deeply by reaching the dermis and subdermal tissues [6, 61]. Blood vessels and nerve endings are destroyed. Finally, a fourth-degree burn affects all layers of the skin, even the muscles. Herein, to confirm the third-degree full-thickness, SD rats were sacrificed at 30 min, 24 h, and 48 h post-burning, and histological analysis of burned tissue was carried out in order to evaluate the burn depth. The results (Fig. 9A) show similar morphological aspects at 30 min and 24 h post-injury, which confirms that burning affected the three skin layers, including the epidermis, dermis, and hypodermis. Additionally, inflammatory cells were observed at 48 h post-burning. All layers of the epidermis were destroyed. Moreover, the dermis, including the papillary dermis and the reticular dermis, as well as their blood vessels, nerve endings, and collagen content, were destroyed. The hypodermis was marked by the presence of damaged adipocytes without nuclei, confirming the full-thickness of the burn wound. However, muscles whose destruction corresponds to the fourth-degree burn remained and did not show any microscopic changes.

3.12.2 Morphology and burn wound closure

The evaluation of burn wound appearance was performed at different time intervals: 0, 2, 5, 7, 10, 14, and 21 days. The morphologic aspects examined were color, border, and consistency. Afterward, the wound healing rate (WHR) was calculated at various time points (Fig. 9C). In each group, the burn wounds were round-shaped and predominantly uniform, with an evident edge separating the wound from unburned skin tissue. The burn wounds were characterized by blisters that appeared within hours post-burning and were examined on day 2. They were filled with a transparent liquid surrounded by a red area (erythema). The treatment of blisters is more or less controversial. Some clinicians report that the blisters act as a protective shield for the burn [64]. Others support the idea that the fluid in the blisters can become infected [64].

Herein, after blister formation, the burn wound was debrided to remove the fluid and extract dead tissue in order to prevent infection (one of the most damning complications in burn victims) by covering the burn wound with the hydrogel with antimicrobial-loaded microsphere. On day 2, there was no significant difference in WHRs

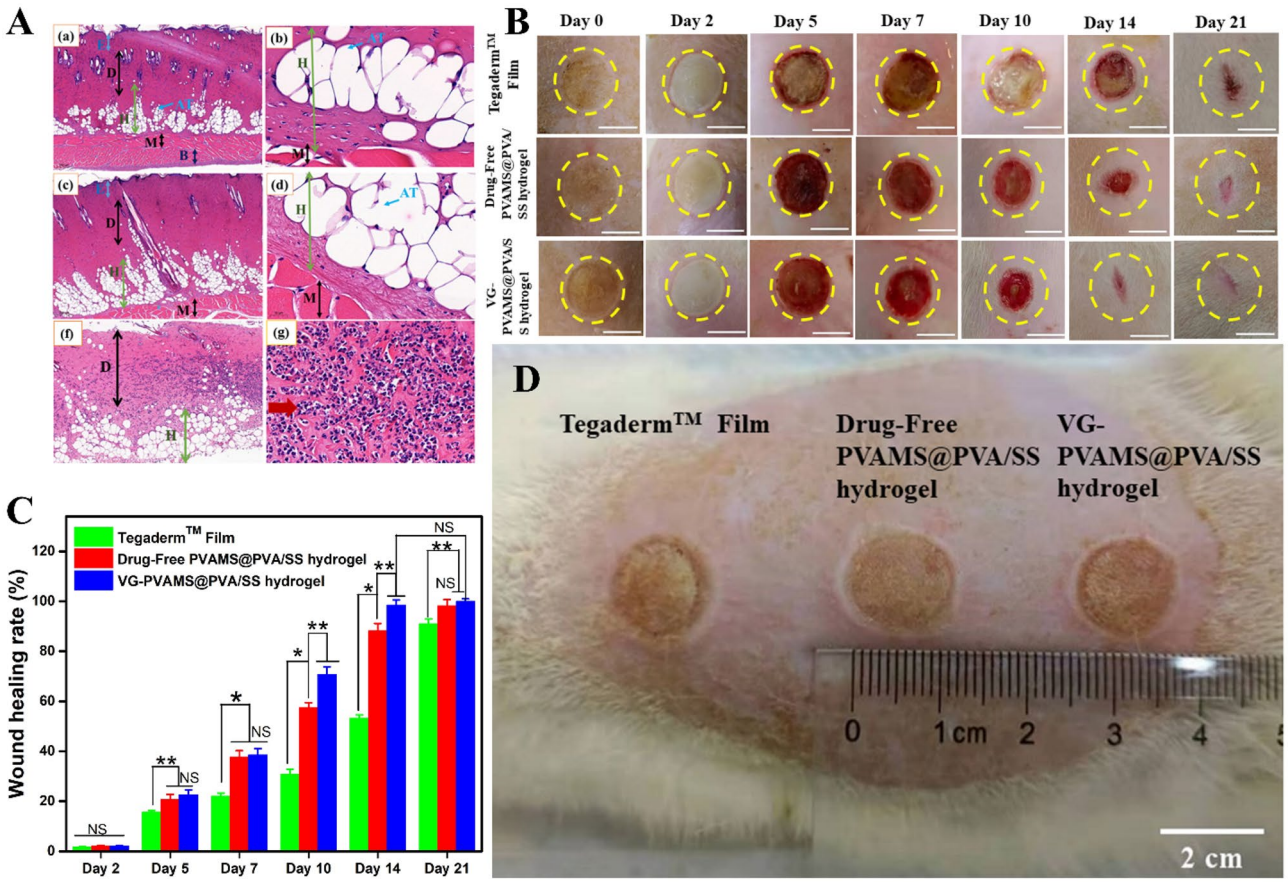

Fig. 9 Burn depth and wound closure analysis. (**A**) Microscopic evaluation of the burn depth on days 0, 1, and 2. (**a**) and (**b**) Burn depth on day 0; (**c**) and (**d**) burn depth on day 1; (**f**) and (**g**) burn depth on day 2 showing neutrophil infiltration. H&E; Magnification: (**a**), (**c**), and (**e**): × 4; (**b**), (**d**), and (**f**): × 40. E: epidermis, D: dermis, H: hypodermis, M: muscle, B: bone, AT: adipose tissue. (**B**) Photographs of burn wounds with different treatment groups on days 0, 2, 5, 7, 10, 14, and 21. (**C**) Burn wound healing rate in different treatment groups at different time points. (**D**) Photocapture of a rat with the different positions of dressing application. NS: no significance, * $P < 0.05$, ** $P < 0.01$

between dressings; relative to initial wound areas, no substantial change was noticeable within the same groups at this point ($P < 0.01$). At days 5 and 7, respectively, the WHR in the drug-free PVAMS-PVA/SS hydrogel (20.6 ± 2.1%, 37.7 ± 2.5%) and VG- PVAMS-PVA/SS (22.2 ± 2.4%, 38.5 ± 2.3%) groups was significantly higher than that in the Tegaderm™ group (15.5 ± 1%, 22.1 ± 1.2%), which could be attributed to the efficient wound healing properties of prepared hydrogels that relied on burst-released SS in the initial stage. On day 10, yellow pus was perceived only in the burn wound bed in the Tegaderm™ group, suggesting the presence of coagulase-negative staphylococci infection confirmed by culturing the pus on an agar plate (Fig. S7A, Supplementary Information) associated with positive catalase (Fig. S7B, Supplementary Information) and negative coagulase (Fig. S7C, Supplementary Information) results. Burns treated with an antimicrobial-free dressing are susceptible to microbial colonization which leads to a prolonged inflammatory phase and the amplified appearance of metalloproteases, causing degeneration of extracellular matrix constituents, slowing the development of new granulation tissue, and consequently reducing the WHR. On day 14, the yellow pus has been reduced, suggesting the effectiveness of the immune system in controlling or reducing the infection.

Interestingly, the WHRs on days 10 and 14 in VG-PVAMS-PVA/SS-treated wounds (70.2 ± 3%, 97.5 ± 2.3%,) were significantly higher than in drug-free PVAMS-PVA/SS (58.2 ± 1.9%, 88.1 ± 3.2%) and Tegaderm™ film (31.2 ± 2%, 53.2 ± 1.4%) groups. Afterward, there was no significant difference between days 14 and 21 in the VG-PVAMS@PVA/SS group, suggesting complete wound closure at day 14, while the drug-free PVAMS@PVA/SS group reached complete wound closure at day 21; at day 21, the Tegaderm™ film only attained 90.9 ± 3.2% wound closure. Generally, from the macroscopic evaluation, it was noticeable that the VG-PVAMS@PVA/SS hydrogel exhibited a more robust capability to accelerate

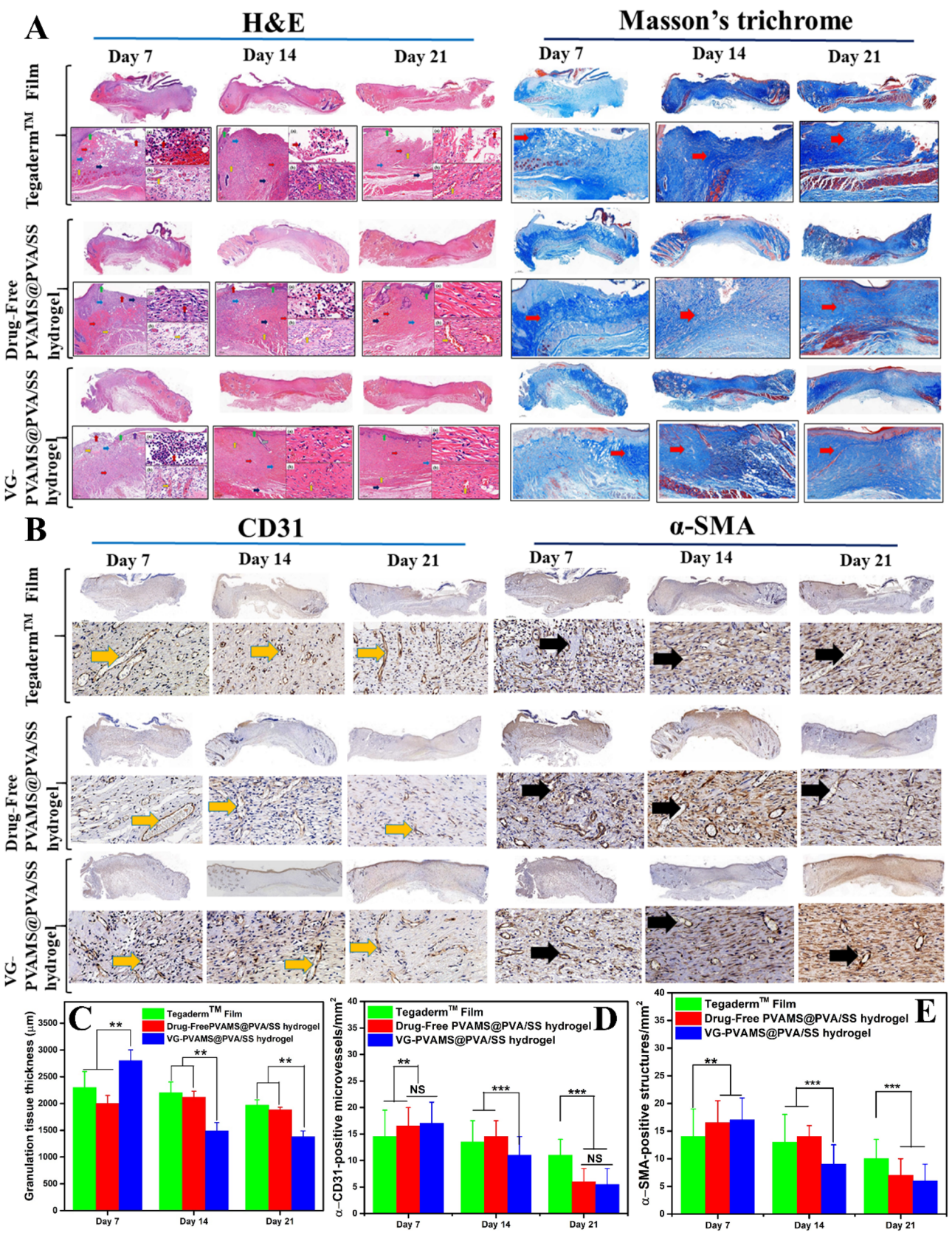
A
H&E
Masson's trichrome
Day 7
Day 14
Day 21
Tegaderm™ Film
Drug-Free PVAMS@PVA/SS hydrogel
VG-PVAMS@PVA/SS hydrogel
B
CD31
α-SMA
C
Granulation tissue thickness (μm)
D
α-CD31-positive microvessels/mm²
E
α-SMA-positive structures/mm²
NS

◂**Fig. 10** Histological analysis of skin wounds. (**A**) H&E and Masson stained sections of skin tissues from treated burn wounds at days 7, 14, and 21. Insert: higher magnification view of the inflammatory cells such as (**a**) neutrophils and (**b**) blood vessels. [H&E; main, × 4; inset, × 30 (**a**); inset, × 80 (**b**)]. (**B**) Images of immunohistochemical staining of CD31 and α-SMA at the burn wound healing sites on days 7, 14, and 21 for the different treatment groups. Scale bar, 50 μm. (**C**) granulation tissue thickness, (**D**) quantification of CD31, and (**E**) α-SMA positive structures/mm^2 on days 7, 14, and 21. Blood vessel (orange arrow), neutrophil (dark red arrow), fibroblast (light blue arrow), collagen (red arrow), keratinocytes (green arrow), adipocytes (dark blue), hair follicle (purple arrow), blood vessel (orange arrow), α-SMA (dark black arrow). NS indicating no significance, *indicating $P < 0.05$, ** indicating $P < 0.01$, and *** indicating $P < 0.001$

burn wound healing and prevent bacterial infection than the drug-free PVAMS@PVA/SS hydrogel and Tegaderm™ film.

3.12.3 Histological analysis of burn wounds

Tissue samples were analyzed by histopathological staining (H&E and trichrome), immunohistochemistry (CK14, CD31, and α-SMA), and immunofluorescence (MPO and MDA) in order to evaluate the therapeutic effect of PVAMS@PVA/SS hydrogel with or without GEN and VA. Inflammatory cells including white blood cells (neutrophils, mastocytes, macrophages, and lymphocytes) were examined to assess the inflammatory phase, blood vessels to assess angiogenesis, and fibroblasts to investigate collagen synthesis.

To evaluate the inflammatory phase, inflammatory cells such as neutrophils in H&E staining (Fig. 10A) and MPO (Fig. 11A) analysis were observed in all groups on day 7, indicating an inflammatory reaction. Neutrophils may increase in response to certain conditions, including burn wounds [65]. When an injury or infectious problem is detected in a tissue, the resident cells secrete chemotactic substances that attract not only the efficient immune cells that circulate in the vessels to supply the damaged tissues, but also control the type of leukocytes recruited according to the chemotactic agents released [65]. Thus, during the inflammatory phase, there is sequential recruitment of the various immune cells. The first cells to be recruited are neutrophils (Fig. 9A), which are attracted by IL-8 produced by endothelial cells and tissue macrophages during the 24 or 48 h following injury or infection. Their early recruitment ensures the arrival of phagocytes immediately after detection of a problem in order to effectively fight against bacterial penetration [65]. The monocytes are recruited in a second step and differentiate into macrophages, which complement the phagocytic action of the neutrophils and also phagocyte the apoptotic bodies derived from the neutrophilic granulocytes. Monocytes can also differentiate into dendritic cells, which take up antigens and migrate to secondary lymphoid organs to present them to lymphocytes and thus trigger an adaptive immune response. Thus, during the inflammatory phase, there is sequential recruitment of the various immune cells. The first cells to be recruited are neutrophils (Fig. 9A), which are attracted by IL-8 produced by endothelial cells and tissue macrophages during the 24 or 48 h following injury or infection. Their early recruitment ensures the arrival of phagocytes immediately after detection of a problem in order to effectively fight against bacterial penetration [65]. The monocytes are recruited in a second step and differentiate into macrophages, which complement the phagocytic action of the neutrophils and also phagocyte the apoptotic bodies derived from the neutrophilic granulocytes. Monocytes can also differentiate into dendritic cells, which take up antigens and migrate to secondary lymphoid organs to present them to lymphocytes and thus trigger an adaptive immune response [66]. The recruitment of inflammatory T cells often indicates the transition from an acute to a chronic inflammatory response [66]. On day 14, there was still the presence of inflammatory cells in the Tegaderm™ film group and in the drug-free PVAMS@PVA/SS hydrogel group, indicating the extension of the inflammatory phase, which further extended the burn healing time. In contrast, no inflammatory cells in H&E and MPO expression were observed on day 14 in the VG-PVAMS@PVA/SS hydrogel group, suggesting good healing performance by shortening the inflammatory phase. On day 21, the number of neutrophils in H&E staining decreased considerably in drug-free PVAMS@PVA/SS and Tegaderm™ film groups, which corresponds to the weak expression of MPO on day 21.

In fact, MPO, which is a reliable indicator of inflammation, participates in the oxidative explosion of certain phagocytes of the immune system, such as neutrophils, and estimates their recruitment and accumulation in burn wound tissue [67]. Furthermore, the results of MDA (Fig. 11A) were in accordance with the results of MPO. In fact, MDA occurs naturally in tissues where it is a manifestation of oxidative cellular stress. It results in particular from the mechanism of action of reactive oxygen derivatives on polyunsaturated fatty acids. MDA has great value in burn wound healing since its high expression delays the healing time. Elevated proinflammatory cytokines released by inflammatory cells are associated with increased reactive oxygen species, resulting in cellular stress [68]. This leads to the vicious cycle where cytokines induce oxidative stress after the stimulation of reduced nicotinamide adenine dinucleotide phosphate (NADPH) through mitochondria, which in turn damages cellular macromolecules and consequently induces inflammation [68]. Therefore, this study demonstrated that controlling the inflammation reaction results in controlling oxidative stress in burn wound healing.

Angiogenesis evaluation was done by H&E staining and the vascular endothelial-specific marker CD31 (Fig. 10B). CD31 is actually staining the central lining of the blood

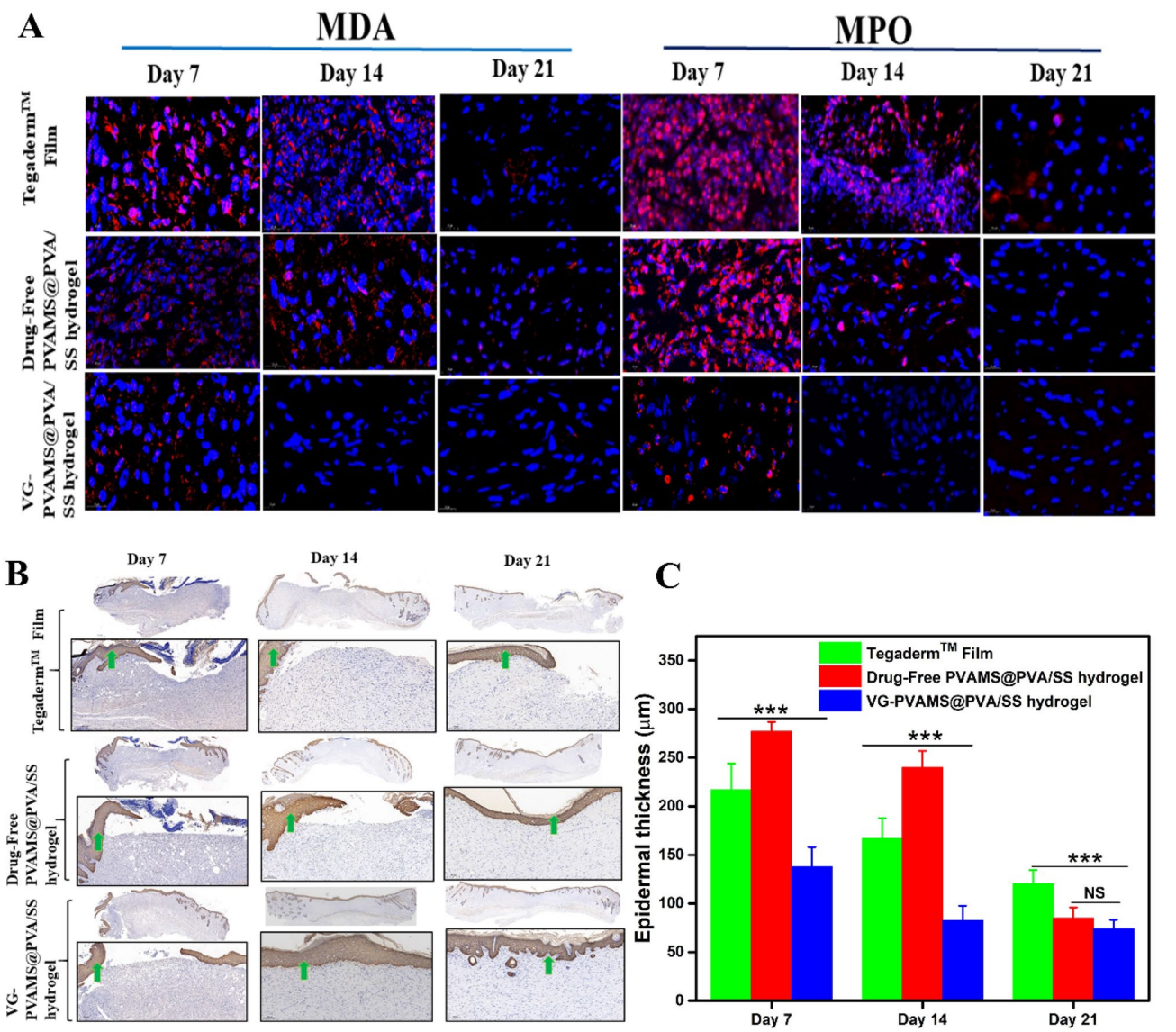

Fig. 11 Immunological analysis of skin wounds. (**A**) Immunofluorescence analysis of MPO and MDA on days 7, 14, and 21. The cells were stained with MPO and MDA in red, and the nuclei were counterstained with DAPI in blue. Scale bar, 20 μm. (**B**) Images of immunohistochemically stained skin tissue for CK14 on days 7, 14, and 21. Scale bar, 50 μm. (**C**) Epidermal thickness of burn skin on days 7, 14, and 21 for the different treated groups

vessel, the lining of the lumen, which is made of endothelial cells, but the muscle wall on the outside is completely negative for CD31 staining [69]. Furthermore, it stains both lymphatics and arteries. Blood vessels were observed in the burn wound site of all groups on day 7, with a higher quantity of blood vessels in VG-PVAMS@PVA/SS (Fig. 10D), suggesting the formation of new blood vessels able to supply nutrients and oxygen, essential for cell proliferation. It was observed that the density of blood vessels decreased with increasing collagen deposition and healing time. The vascular smooth muscle cells' marker α-SMA expression was analogous to that of CD31 (Fig. 10E). In the skin, α-SMA is either in the blood vessel walls or in the arrector pili muscles. α-SMA correlates with the activation of fibroblasts for scar-producing myofibroblasts.

Collagen synthesized by fibroblasts on day 7 was detected by Masson trichrome staining in all groups (Fig. 10A). The collagen deposition was progressively increased with increasing burn healing time for all groups. The arrangement of collagen fibers performs a crucial function throughout the remodeling phase and, therefore, on the final scar formation after burn wound closure [70]. Herein, the burn wound heals without scarring, suggesting a good orientation and arrangement of collagen fibers. Additionally, the thickness of the granulation tissue decreased with increasing wound healing time in all groups (Fig. 10C).

Furthermore, Cytokeratin, an intermediate filament-building protein that fills up epithelial cells of all sorts, was evaluated [71]. So the dark brown color in Fig. 11B highlights the epidermis, whereas the dermis, which is made of collagen, is totally negative for keratin, but the hair follicles and sweat glands, also made of epithelium, are also keratin-positive. On day 14, more CK14 expression in the VG-PVAMS@PVA/SS hydrogel group highlighted the complete re-epithelization, while the drug-free PVAMS@PVA/SS group achieved high expression of CK14 on day 21. However, the expression of CK14 in the burn wound site was impaired due to the lower healing ability in the Tegaderm™ film group. In addition, we quantified the epidermal thickness in different groups at various time points. As illustrated in Fig. 11C, the epidermal thickness decreased with rising burn healing time for all treatment groups. On day 14, the VG-PVAMS@PVA/SS group displayed thinner epidermal thickness than other groups, signifying its rapid wound healing effects.

Taking all of the above findings into account, we deduce that the VG-PVAMS@PVA/SS hydrogel provided an excellent sterile scaffold for promoting infected burn wound healing.

4 Conclusion

Multidrug resistance (MDR) is considered a problem that impairs burn wound healing. The combination of antibiotics exhibiting synergistic effects proved to be very efficient against MDR bacteria involved in burn wound infections. In the present study, PVA microspheres containing VA and GEN prepared by inverse emulsion crosslinking were incorporated into a PVA/SS pre-gel which was further freeze-thawed to obtain bioactive hydrogel embedding microspheres. High GEN and VA concentrations above MIC were released from the constructs with zero-order kinetics without an initial burst release, leading to bacterial growth inhibition (MRSA*, P. aeruginosa,* and *E. coli)* without the occurrence of tolerance. Moreover, the samples displayed long-term swelling behavior and thermal stability, with the average diameter of microspheres, the pore size, and the porosity required for parenteral injection as well as skin regeneration. Rheological analysis showed that the loaded hydrogel showed injectability with the potential for recoverability when undergoing discontinued shear strain, which makes it suitable for deep burn wound management. The addition of drugs to the hydrogel did not affect the biocompatibility of PVA and SS. Additionally, SS released at a non-constant rate enhanced cell viability, supporting the extracellular matrix-like behavior of the samples as to cell growth. Furthermore, the *in vitro* hemolysis test showed that the hydrogels did not show any drug-induced hemolysis. *In vivo* results showed that the release of SS, VA, and GEN from PVAMS embedded in the microporous hybrid hydrogel accelerated the burn wound healing and prevented scar formation. Thus, VG-PVAMS@PVA/SS hydrogel is a very promising and advanced topical injectable gel for the treatment of infected burn wounds, which further has the advantage of parental drug delivery. This study opens novel avenues for the treatment of burn wound infection by local injection of antibiotic combination-loaded hydrogel or antibiotic hybrid-loaded hydrogel. Nevertheless, further clinical investigations are suggested to support the effectiveness allegations in humans.

Supplementary Information The online version contains supplementary material available at https://doi.org/10.1007/s42114-022-00467-6.

Acknowledgements The authors sincerely thank the Analysis and Test Center at Huazhong University of Science and Technology for the related characterizations of various samples.

Funding This work was financially supported by the National Natural Science Foundation of China (51973076); BRICS STI Framework Programme 3rd call 2019, the National Key Research and Development Program of China (2018YFE0123700); and the Fundamental Research Funds for the Central Universities (2020kfyXJJS035).

Declarations

Conflicts of Interest The authors declare that they have no conflict of interest.

References

1. Mestrallet G, Rouas-Freiss N, LeMaoult J et al (2021) Skin immunity and tolerance: focus on epidermal keratinocytes expressing HLA-G. Front Immunol 12:772516. https://doi.org/10.3389/fimmu.2021.772516
2. Ladhani HA, Yowler CJ, Claridge JA (2021) Burn wound colonization, infection, and sepsis. Surg Infect 22:44–48. https://doi.org/10.1089/sur.2020.346
3. Church D, Elsayed S, Reid O et al (2006) Burn wound infections. Clin Microbiol Rev 19:403–434. https://doi.org/10.1128/CMR.19.2.403-434.2006
4. Azevedo MM, Pina-Vaz C, Rodrigues AG (2021) The role of phage therapy in burn wound infections management: advantages and pitfalls. J Burn Care Res. https://doi.org/10.1093/jbcr/irab175
5. Chen Y-Y, Wu P-F, Chen C-S et al (2020) Trends in microbial profile of burn patients following an event of dust explosion at a tertiary medical center. BMC Infect Dis 20:193. https://doi.org/10.1186/s12879-020-4920-4
6. Vinaik R, Barayan D, Shahrokhi S, Jeschke MG (2019) Management and prevention of drug resistant infections in burn patients. Expert Rev Anti Infect Ther 17:607–619. https://doi.org/10.1080/14787210.2019.1648208
7. Shu W, Wang Y, Zhang X et al (2021) Functional hydrogel dressings for treatment of burn wounds. Front Bioeng Biotechnol 9:788461. https://doi.org/10.3389/fbioe.2021.788461
8. Zhang X, Shu W, Yu Q et al (2020) Functional biomaterials for treatment of chronic wound. Front Bioeng Biotechnol 8:516. https://doi.org/10.3389/fbioe.2020.00516

9. Moorcroft SCT, Roach L, Jayne DG et al (2020) Nanoparticle-loaded hydrogel for the light-activated release and photothermal enhancement of antimicrobial peptides. ACS Appl Mater Interfaces 12:24544–24554. https://doi.org/10.1021/acsami.9b22587
10. Zhou K, Wang M, Zhou Y et al (2022) Comparisons of antibacterial performances between electrospun polymer@drug nanohybrids with drug-polymer nanocomposites. Adv Compos Hybrid Mater. https://doi.org/10.1007/s42114-021-00389-9
11. Yu D, Wang M, Ge R (2021) Strategies for sustained drug release from electrospun multi-layer nanostructures. Wiley Interdiscip Rev Nanomed Nanobiotechnol. https://doi.org/10.1002/wnan.1772
12. Liu X, Xu H, Zhang M, Yu D-G (2021) Electrospun medicated nanofibers for wound healing: Review. Membranes (Basel) 11:770. https://doi.org/10.3390/membranes11100770
13. Zhang M, Song W, Tang Y et al (2022) Polymer-based nanofiber–nanoparticle hybrids and their medical applications. Polymers (Basel) 14:351. https://doi.org/10.3390/polym14020351
14. Rukavina Z, Šegvić Klarić M, Filipović-Grčić J et al (2018) Azithromycin-loaded liposomes for enhanced topical treatment of methicillin-resistant Staphyloccocus aureus (MRSA) infections. Int J Pharm 553:109–119
15. Chen N, Wang H, Ling C et al (2019) Cellulose-based injectable hydrogel composite for pH-responsive and controllable drug delivery. Carbohydr Polym 225:115207. https://doi.org/10.1016/j.carbpol.2019.115207
16. Chen X, Xu C, He H (2019) Electrospinning of silica nanoparticles-entrapped nanofibers for sustained gentamicin release. Biochem Biophys Res Commun 516:1085–1089
17. Kircik LH (2011) Microsphere technology: hype or help? J Clin Aesthet Dermatol 4:27–31
18. Wang M, Huang X, Zheng H et al (2021) Nanomaterials applied in wound healing: mechanisms, limitations and perspectives. J Control Release 337:236–247. https://doi.org/10.1016/j.jconrel.2021.07.017
19. Malamatari M, Charisi A, Malamataris S et al (2020) Spray drying for the preparation of nanoparticle-based drug formulations as dry powders for inhalation. Processes 8:788. https://doi.org/10.3390/pr8070788
20. Hiremath L, Sruti O, Aishwarya BM et al (2021) Electrospun nanofibers: characteristic agents and their applications. In: Kumar B (ed) Nanofibers - Synthesis, Properties and Applications. IntechOpen
21. Bayer IS (2021) A review of sustained drug release studies from nanofiber hydrogels. Biomedicines 9:1612. https://doi.org/10.3390/biomedicines9111612
22. Li W, Chen J, Zhao S et al (2022) High drug-loaded microspheres enabled by controlled in-droplet precipitation promote functional recovery after spinal cord injury. Nat Commun 13:1262. https://doi.org/10.1038/s41467-022-28787-7
23. Saini S, Kumar S, Choudhary M, Budhwar V (2018) Microspheres as controlled drug delivery system: an updated review. Int J Pharm Sci 9:1760. https://doi.org/10.13040/IJPSR.0975-8232.9(5).1760-68
24. Saralidze K, Koole LH, Knetsch MLW (2010) Polymeric microspheres for medical applications. Materials (Basel) 3:3537–3564. https://doi.org/10.3390/ma3063537
25. Mok CF, Ching YC, Muhamad F et al (2020) Adsorption of dyes using poly(vinyl alcohol) (pva) and PVA-based polymer composite adsorbents: a review. J Polym Environ 28:775–793. https://doi.org/10.1007/s10924-020-01656-4
26. Lamboni L, Gauthier M, Yang G, Wang Q (2015) Silk sericin: A versatile material for tissue engineering and drug delivery. Biotechnol Adv 33:1855–1867. https://doi.org/10.1016/j.biotechadv.2015.10.014
27. Boni BOO, Lamboni L, Bakadia BM et al (2020) Combining silk sericin and surface micropatterns in bacterial cellulose dressings to control fibrosis and enhance wound healing. Eng Sci. https://doi.org/10.30919/es8d906
28. Mazer-Amirshahi M, Pourmand A, May L (2017) Newly approved antibiotics and antibiotics reserved for resistant infections: Implications for emergency medicine. Am J Emerg Med 35:154–158. https://doi.org/10.1016/j.ajem.2016.10.034
29. Domalaon R, Idowu T, Zhanel GG, Schweizer F (2018) Antibiotic hybrids: the next generation of agents and adjuvants against gram-negative pathogens? Clin Microbiol Rev 31:e00077-e117. https://doi.org/10.1128/CMR.00077-17
30. Ng VWL, Chan JMW, Sardon H et al (2014) Antimicrobial hydrogels: A new weapon in the arsenal against multidrug-resistant infections. Adv Drug Deliv Rev 78:46–62. https://doi.org/10.1016/j.addr.2014.10.028
31. Worthington RJ, Melander C (2013) Combination approaches to combat multidrug-resistant bacteria. Trends Biotechnol 31:177–184. https://doi.org/10.1016/j.tibtech.2012.12.006
32. Gupta V, Datta P (2019) Next-generation strategy for treating drug resistant bacteria: Antibiotic hybrids. Indian J Med Res 149:97–106. https://doi.org/10.4103/ijmr.IJMR_755_18
33. Simner PJ, Patel R (2020) Cefiderocol antimicrobial susceptibility testing considerations: the achilles' heel of the trojan horse? J Clin Microbiol 59:e00951-e1020. https://doi.org/10.1128/JCM.00951-20
34. Cong Y, Yang S, Rao X (2020) Vancomycin resistant Staphylococcus aureus infections: A review of case updating and clinical features. J Adv Res 21:169–176. https://doi.org/10.1016/j.jare.2019.10.005
35. Sidrim JJC, Teixeira CEC, Cordeiro RA et al (2015) β-Lactam antibiotics and vancomycin inhibit the growth of planktonic and biofilm Candida spp.: An additional benefit of antibiotic-lock therapy? Int J Antimicrob Agents 45:420–423. https://doi.org/10.1016/j.ijantimicag.2014.12.012
36. Bakadia BM, Souho T, Lamboni L et al (2021) Types and transmission routes of nosocomial antibacterial resistance. IJMSHR 5:156–168. https://doi.org/10.51505/IJMSHR.2021.5115
37. Ionita D, Bajenaru-Georgescu D, Totea G et al (2017) Activity of vancomycin release from bioinspired coatings of hydroxyapatite or TiO2 nanotubes. Int J Pharm 517:296–302. https://doi.org/10.1016/j.ijpharm.2016.11.062
38. Lamboni L, Li Y, Liu J, Yang G (2016) Silk sericin-functionalized bacterial cellulose as a potential wound-healing biomaterial. Biomacromol 17:3076–3084. https://doi.org/10.1021/acs.biomac.6b00995
39. Tam VH, Kabbara S, Vo G et al (2006) Comparative pharmacodynamics of gentamicin against Staphylococcus aureus and Pseudomonas aeruginosa. Antimicrob Agents Chemother 50:2626–2631. https://doi.org/10.1128/AAC.01165-05
40. Masi M, Réfregiers M, Pos KM, Pagès JM (2017) Mechanisms of envelope permeability and antibiotic influx and efflux in Gram-negative bacteria. Nat Microbiol 2:28224989. https://doi.org/10.1038/nmicrobiol.2017.1
41. Muheim C, Götzke H, Eriksson AU et al (2017) Increasing the permeability of Escherichia coli using MAC13243. Sci Rep 7:1–11. https://doi.org/10.1038/s41598-017-17772-6
42. Ahmadi K, Hashemian AM, Bolvardi E, Hosseini PK (2016) vancomycin-resistant Pseudomonas aeroginosa in the cases of trauma. Med Arch 70:57–60. https://doi.org/10.5455/medarh.2016.70.57-60
43. Zhou A, Kang TM, Yuan J et al (2015) Synergistic interactions of vancomycin with different antibiotics against escherichia coli: Trimethoprim and nitrofurantoin display strong synergies with vancomycin against wild-type E. coli. Antimicrob Agents Chemother 59:276–281. https://doi.org/10.1128/AAC.03502-14

44. Miquel S, Lagrafeuille R, Souweine B, Forestier C (2016) Anti-biofilm activity as a health issue. Front Microbiol 7:1–14. https://doi.org/10.3389/fmicb.2016.00592
45. Gohil JM, Bhattacharya A, Ray P (2006) Studies on the cross-linking of poly (vinyl alcohol). J Polym Res 13:161–169. https://doi.org/10.1007/s10965-005-9023-9
46. Stoica-Guzun A, Stroescu M, Jipa I et al (2013) Effect of γ irradiation on poly(vinyl alcohol) and bacterial cellulose composites used as packaging materials. Radiat Phys Chem 84:200–204. https://doi.org/10.1016/j.radphyschem.2012.06.017
47. Thum J-Y, Sin LT, Bee S-T et al (2022) Investigation of calcination of sepia officinalis cuttlefish bone for reinforcement of polyvinyl alcohol added nano-size montmorillonite. Polymers (Basel) 14:1089. https://doi.org/10.3390/polym14061089
48. Danaei M, Dehghankhold M, Ataei S et al (2018) Impact of particle size and polydispersity index on the clinical applications of lipidic nanocarrier systems. Pharmaceutics 10:57. https://doi.org/10.3390/pharmaceutics10020057
49. Mao S, Guo C, Shi Y, Li LC (2012) Recent advances in polymeric microspheres for parenteral drug delivery – part 1. Expert Opin Drug Deliv 9:1161–1176. https://doi.org/10.1517/17425247.2012.709844
50. Enrione J, Char C, Pepczynska M et al (2020) Rheological and structural study of salmon gelatin with controlled molecular weight. Polymers (Basel) 12:1587. https://doi.org/10.3390/polym12071587
51. Seong Y-J, Lin G, Kim BJ et al (2019) Hyaluronic acid-based hybrid hydrogel microspheres with enhanced structural stability and high injectability. ACS Omega 4:13834–13844. https://doi.org/10.1021/acsomega.9b01475
52. Kim KK, Pack DW (2006) Microspheres for drug delivery. BioMEMS and Biomedical Nanotechnology. Springer, US, Boston, MA, pp 19–50
53. Schwendeman SP, Shah RB, Bailey BA, Schwendeman AS (2014) Injectable controlled release depots for large molecules. J Control Release 190:240–253. https://doi.org/10.1016/j.jconrel.2014.05.057
54. Champion JA, Walker A, Mitragotri S (2008) Role of particle size in phagocytosis of polymeric microspheres. Pharm Res 25:1815–1821. https://doi.org/10.1007/s11095-008-9562-y
55. Nosrati H, Aramideh Khouy R, Nosrati A et al (2021) Nanocomposite scaffolds for accelerating chronic wound healing by enhancing angiogenesis. J Nanobiotechnology 19:1. https://doi.org/10.1186/s12951-020-00755-7
56. Loh QL, Choong C (2013) Three-dimensional scaffolds for tissue engineering applications: role of porosity and pore size. Tissue Eng Part B Rev 19:485–502. https://doi.org/10.1089/ten.teb.2012.0437
57. Jeschke MG, van Baar ME, Choudhry MA et al (2020) Burn injury. Nat Rev Dis Prim 6:11. https://doi.org/10.1038/s41572-020-0145-5
58. Amalraj A, Raj KKJ, Haponiuk JT et al (2020) Preparation, characterization, and antimicrobial activity of chitosan/gum arabic/polyethylene glycol composite films incorporated with black pepper essential oil and ginger essential oil as potential packaging and wound dressing materials. Adv Compos Hybrid Mater 3:485–497. https://doi.org/10.1007/s42114-020-00178-w
59. Hassan CM, Peppas NA (2000) Structure and morphology of freeze/thawed PVA hydrogels. Macromolecules 33:2472–2479. https://doi.org/10.1021/ma9907587
60. Sirousazar M, Kokabi M, Hassan ZM (2012) Swelling behavior and structural characteristics of polyvinyl alcohol/montmorillonite nanocomposite hydrogels. J Appl Polym Sci 123:50–58. https://doi.org/10.1002/app.34437
61. Mofazzal Jahromi MA, Sahandi Zangabad P, Moosavi Basri SM et al (2018) Nanomedicine and advanced technologies for burns: Preventing infection and facilitating wound healing. Adv Drug Deliv Rev 123:33–64. https://doi.org/10.1016/j.addr.2017.08.001
62. Chen J, Zhang G, Zhao Y et al (2022) Promotion of skin regeneration through co-axial electrospun fibers loaded with basic fibroblast growth factor. Adv Compos Hybrid Mater. https://doi.org/10.1007/s42114-022-00439-w
63. Solarte David VA, Güiza-Argüello VR, Arango-Rodríguez ML et al (2022) Decellularized tissues for wound healing: towards closing the gap between scaffold design and effective extracellular matrix remodeling. Front Bioeng Biotechnol 10:821852. https://doi.org/10.3389/fbioe.2022.821852
64. Murphy F, Amblum J (2014) Treatment for burn blisters: debride or leave intact? Emerg Nurse 22:24–27. https://doi.org/10.7748/en2014.04.22.2.24.e1300
65. de Oliveira S, Rosowski EE, Huttenlocher A (2016) Neutrophil migration in infection and wound repair: going forward in reverse. Nat Rev Immunol 16:378–391. https://doi.org/10.1038/nri.2016.49
66. Janakiram NB, Valerio MS, Goldman SM, Dearth CL (2021) The role of the inflammatory response in mediating functional recovery following composite tissue injuries. Int J Mol Sci 22:13552. https://doi.org/10.3390/ijms222413552
67. Davies MJ, Hawkins CL (2020) The role of myeloperoxidase in biomolecule modification, chronic inflammation, and disease. Antioxid Redox Signal 32:957–981. https://doi.org/10.1089/ars.2020.8030
68. Bakadia BM, Boni BOO, Ahmed AAQ, Yang G (2021) The impact of oxidative stress damage induced by the environmental stressors on COVID-19. Life Sci 264:118653. https://doi.org/10.1016/j.lfs.2020.118653
69. Park SH, Cho A, Ryu HJ, Kim H (2022) Profile of vascular markers and CT enhancement of hyaline vascular type castleman's disease. Microvasc Res 142:104357. https://doi.org/10.1016/j.mvr.2022.104357
70. Mathew-Steiner SS, Roy S, Sen CK (2021) Collagen in wound healing. Bioengineering 8:63. https://doi.org/10.3390/bioengineering8050063
71. Kuburich NA, den Hollander P, Pietz JT, Mani SA (2021) Vimentin and cytokeratin: good alone, bad together. Semin Cancer Biol. https://doi.org/10.1016/j.semcancer.2021.12.006

Authors and Affiliations

Bianza Moise Bakadia[1,2] · Aimei Zhong[3] · Xiahong Li[4] · Biaou Oscar Ode Boni[1] · Abeer Ahmed Qaed Ahmed[5] · Tiatou Souho[6] · Ruizhu Zheng[1] · Zhijun Shi[1] · Dingwen Shi[8] · Lallepak Lamboni[1,7] · Guang Yang[1]

✉ Lallepak Lamboni
lallepak@yahoo.fr

✉ Guang Yang
yang_sunny@yahoo.com

1 Department of Biomedical Engineering, College of Life Science and Technology, Huazhong University of Science and Technology, Wuhan 430074, China

2 Institut Superieur des Techniques Medicales de Lubumbashi, Lubumbashi, Democratic Republic of the Congo

3 Department of Plastic Surgery, Union Hospital, Tongji Medical College, Huazhong University of Science and Technology, Wuhan, Hubei, China

4 State Key Laboratory of High Performance Ceramics and Superfine Microstructure, Shanghai Institute of Ceramics, Chinese Academy of Sciences, Shanghai 200050, China

5 Department of Environmental Sciences, School of Agriculture and Environmental Sciences, University of South Africa, P.O. Box 392, Florida, Johannesburg 1710, South Africa

6 Département Des Sciences de La Vie Et de La Terre, Faculté Des Sciences Et Techniques, Université de Kara, Kara, Togo

7 Laboratoire de Biologie Moléculaire Et Virologie, Institut National d'Hygiène-Togo, 26 Rue Nangbéto, Quartier Administratif, PO Box 1396, Lomé, Togo

8 College of Life Science and Technology, National Engineering Research Center for Nanomedicine, Huazhong University of Science and Technology, Wuhan City 430074, China